International Journal of Fatigue 103 (2017) 557–575

Contents lists available at ScienceDirect

International Journal of Fatigue

journal homepage: www.elsevier.com/locate/ijfatigue

Using the strip-yield mechanics to model fatigue crack growth by damage accumulation ahead of the crack tip

Samuel Elias Ferreira, Jaime Tupiassú Pinho de Castro *, Marco Antonio Meggiolaro

Mechanical Engineering Department, PUC-Rio, Brazil

ARTICLE INFO

Article history:
Received 22 December 2016
Received in revised form 15 June 2017
Accepted 28 June 2017
Available online 30 June 2017

Keywords:
Fatigue crack growth models
Strip-yield mechanics
Crack closure
Damage accumulation ahead of the crack tip

ABSTRACT

Elber found in the early 70s that fatigue cracks can close under tensile loads, and assumed that fatigue crack growth (FCG) would be controlled by $\Delta K_{eff} = K_{max} - K_{op}$, where K_{max} and K_{op} are the maximum and opening values of the stress intensity factor. This hypothesis can rationalize many transient effects observed under service loads, but it cannot explain many other effects like FCG retardation or arrest after overloads under high $R = K_{min}/K_{max}$, when $K_{min} > K_{op}$; FCG at constant rates under highly variable ΔK_{eff}; cracks arrested at a given R that can reinitiate to grow at a lower R without changing their ΔK_{eff}; or the R-insensitivity of FCG in inert environments. Nevertheless, strip-yield models (SYM) based on ΔK_{eff} ideas are more used for FCG life predictions than alternative models based on any other principles. To verify whether SYMs are indeed intrinsically better, their mechanics is used to predict FCG rates based both on Elber's ideas and on the alternative view that FCG is instead due to damage accumulation ahead of the crack tip, which does not need the ΔK_{eff} hypothesis or arbitrary data-fitting parameters. Despite based on conflicting principles, both models can reproduce quite well FCG data obtained under quasi-constant ΔK loading, a somewhat surprising result that deserves to be carefully analyzed.

1. Introduction

Paris and Erdogan demonstrated in 1963 that stable fatigue crack growth (FCG) rates da/dN can be correlated with stress intensity factor (SIF) ranges ΔK, at least in the central region of typical $da/dN \times \Delta K$ curves, where their $da/dN = A \cdot \Delta K^m$ rule applies [1]. Since then, many other rules have been proposed to better fit the FCG behavior, quantifying the effect of other parameters that can affect FCG rates as well, such as the peak load K_{max} or the load ratio $R = K_{min}/K_{max}$, FCG thresholds $\Delta K_{th}(R)$, and fracture toughness K_c [2]. In particular, after discovering plasticity-induced crack closure (PICC) under tension loads in 1970, Elber postulated that fatigue damage can only be induced after the crack tip is completely opened, under loads $K > K_{op}$, where K_{op} is the crack opening load [3,4]. His $da/dN = f(\Delta K_{eff} = K_{max} - K_{op})$ hypothesis can plausibly rationalize many peculiarities of the FCG behavior, such as crack growth delays and arrests after overloads (OL), reductions on OL-induced delays after underloads (UL), or the trend of the R-dependence of FCG thresholds, so important to estimate fatigue lives under variable amplitude loads (VAL). Hence, his ΔK_{eff} idea has been used in many semi-empirical FCG models, among them the so-called strip-yield models (SYMs) that estimate opening loads from the residual strains that surround the crack faces and FCG lives using a suitable $da/dN \times \Delta K_{eff}$ equation properly fitted to experimental data [5–9].

Many works support the $da/dN = f(\Delta K_{eff})$ hypothesis, as extensively reviewed e.g. by Kemp [10] and by Skorupa [11,12], but many others question it. A few examples of FCG behaviors that cannot be explained by Elber's postulate are: FCG delays or arrests after OLs under high R, when $K_{min} > K_{op}$ [13]; constant FCG rates induced by fixed $\{\Delta K, R\}$, but highly variable ΔK_{eff} loadings [14]; cracks arrested at a given R that reinitiate to grow at a lower R under the same ΔK_{eff} [16]; or the R-insensitivity of FCG in inert environments [17]. Still other questions about the ΔK_{eff} hypothesis are explored in [18–23]. Even though this work does not aim to support or to refute Elber's idea, or to review the works that support or question it, it can be claimed that without doubt this idea still remains controversial.

In view of such doubts, the goal of this work is to first use well-proven strip-yield mechanics [5–9] to describe some carefully measured $da/dN \times \Delta K$ curves at low and high R. However, instead of simply assuming that a reasonable fit of some properly measured data is an undisputable proof that the ΔK_{eff} hypothesis is valid, the very same strip-yield mechanics is here used to verify whether another hypothesis about the cause for the FCG process

* Corresponding author.
E-mail address: jtcastro@puc-rio.br (Jaime Tupiassú Pinho de Castro).

http://dx.doi.org/10.1016/j.ijfatigue.2017.06.039
0142-1123/

Nomenclature

a	crack length
b	fatigue strength exponent
b_k	dimensions for a partially loaded crack (k = 1, 2) (m)
c	fatigue ductility exponent
C	coefficient of the critical damage crack growth rate equation
C_n	coefficient of the NASGRO crack growth rate equation
CAL	constant amplitude loading
CDM	critical damage model
CTOD	crack-tip opening displacement
d	half length of the crack plus the monotonic plastic zone (m)
$D(i)$	accumulated damage at each ith element ahead of the crack tip
da/dN	fatigue crack growth rate
E	Young's modulus of elasticity (MPa)
EP	elastoplastic
FCG	fatigue crack growth
h	Ramberg-Osgood strain-hardening exponent
h_c	Ramberg-Osgood cyclic strain-hardening exponent
H_c	Ramberg-Osgood cyclic strain-hardening coefficient (MPa)
HRR	Hutchinson, Rice and Rosengren stress and strain fields
K	stress intensity factor, SIF (MPa$\sqrt{}$m)
K_c	fracture toughness, and its value under plane strain conditions (MPa$\sqrt{}$m)
$K_{\max}$	maximum stress intensity factor (MPa$\sqrt{}$m)
$K_{\min}$	minimum stress intensity factor (MPa$\sqrt{}$m)
K_{op}	crack opening stress intensity factor (MPa$\sqrt{}$m)
K_{res}	residual stress intensity factor (MPa$\sqrt{}$m)
K_t	stress concentration factor
LE	linear elastic
L_i	length of the element i created by plastic deformation (m)
n	total number of bar elements
n_i	number of applied load cycles
N_i	fatigue life under CAL conditions
n_{pz}	number of elements in the plastic zone
OL	overload
PICC	plasticity induced crack closure
pz	plastic zone
pz_r	reverse (or cyclic) plastic zone
r	distance from crack tip, radial coordinate
rl	residual ligament of the element where the crack tip stops after each load cycle
R	load ratio ($\sigma_{\min}/\sigma_{\max}$ or $K_{\min}/K_{\max}$)
R_x	capped load ratio ($R_x = R$ if $R > 0$ and $R_x = 0$ if $R \leq 0$)
S_F	flow strength, $S_F = (S_Y + S_U)/2$ (MPa)
SIF	stress intensity factor
S_U	ultimate strength (MPa)
S_Y	yield strength (MPa)
S_{Yc}	cyclic yield strength (MPa)
SY-CDM	combined strip-yield critical-damage model
SYM	strip-yield model
t	specimen thickness (m)
UL	underload
V	crack surface displacement (m)
VAL	variable amplitude loading
VE	volume element
W	specimen half-width (m)
w_i	half-width of bar element i (m)
x, y	Cartesian coordinates
$x(i)$	coordinate location of the element i starting from the specimen center (m)
$x_{ct}(i)$	coordinate location starting from the current crack tip (m)
X	displacement of the HRR strain field (m)
α	constraint factor: $\alpha = 1$ for plane stress; $\alpha = 3$ for plane strain
Δa^*	crack growth increment over which S_o is held constant (m)
ΔN	number of load cycles to growth the crack by an increment Δc^*
ΔK	stress intensity factor range (MPa$\sqrt{}$m)
ΔK_{eff}	effective stress intensity factor range (MPa$\sqrt{}$m)
ΔK_0	effective threshold stress intensity factor range (MPa$\sqrt{}$m)
ΔK_{th}	threshold stress intensity factor range (MPa$\sqrt{}$m)
Δ_c	width of the volume element in the Critical Damage Model, CDM (m)
$\Delta\varepsilon_y$	strain range in the y direction (m/m)
ε_c	Coffin-Manson's fatigue ductility coefficient
η	material constant, $\eta = 0$ for plane stress and $\eta = \nu$ for plane strain
ν	Poisson's ratio
ρ	crack tip radius (m)
ρ^*	elementary material block size from UniGrow's model (m)
σ_c	Coffin-Manson's fatigue strength coefficient (MPa)
σ_j	stress at a segment of the crack surface (MPa)
σ_{op}	crack opening stress (MPa)
σ_m	mean applied stress (MPa)
$\sigma_{\max}$, $\sigma_{\min}$	maximum and minimum applied stress (MPa)

can be equally used to fit the same data. To do so, this mechanics is used to verify the alternative view that the FCG process, instead of controlled by ΔK_{eff}, can be due to damage accumulation ahead of the crack tip, assuming fatigue cracks advance by sequentially breaking small volume elements (VE) adjacent to the tip after they reach the critical damage the material can sustain. If properly applied, this alternative hypothesis neither needs the ΔK_{eff} hypothesis, nor requires arbitrary data-fitting parameters [13,24–26].

Somewhat surprisingly, this exercise shows that both models, although based on contradictory hypotheses, can reproduce quite well the FCG data analyzed here. Therefore, it demonstrates that conflicting views about the *cause* for the FCG process can be equally used to model $da/dN \times \Delta K$ curves using the very same basic mechanics! Such a conclusion indicates that radical opinions such as "all FCG problems can be modeled by ΔK_{eff} concepts "or" ΔK_{eff} concepts are useless to model FCG" are at least questionable. It also indicates that what really is a "conclusive proof criterion" in this topic should be reevaluated. The models used to support this claim are briefly reviewed next.

2. Critical damage models

Critical Damage Models (CDMs) assume fatigue cracks grow by damage accumulation at the uncracked ligament ahead of their tips due to cyclic elastoplastic (EP) stress/strains histories that act there [13,24–30]. If this is so, most of the fatigue damage occurs inside the reverse or cyclic plastic zones (pz_r) that always follow fatigue crack tips. This way, CDMs suppose fatigue cracks grow by sequentially breaking small volume elements (VE) adjacent to

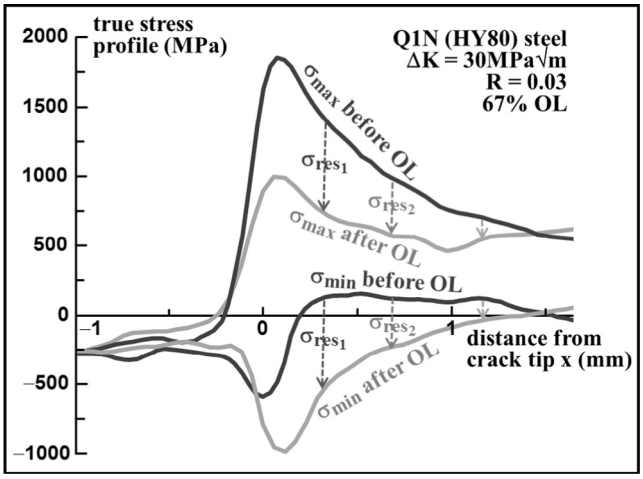

Fig. 1. Stress profiles behind ($x < 0$) and ahead of ($x > 0$) a fatigue crack tip at K_{max} and K_{min} baseline loads, before an OL and 40 cycles after it, measured by Withers et al. using tomography techniques [33]. Notice how the σ_{max} and σ_{min} stress profiles ahead of the crack tip are *both* reduced by roughly the same values due to the OL-induced residual stresses.

their tips that reach the critical damage the material can sustain. Such VE are analogous to tiny εN specimens that see VAL during their lives even under constant amplitude loadings (CAL), since both $\Delta\varepsilon$ and σ_{max} increase as the crack tip approaches them. Some CDMs consider the width of the VE as the distance that the crack grows at each load cycle [24–27]. Others consider the FCG rate as being an arbitrary VE width divided by the number of cycles that the crack needs to cross it [29,30].

The UniGrow model is a recent CDM that uses numerical tools to evaluate the EP stress/strain history ahead of the crack tip [30]. It assumes that FCG is driven by ΔK and K_{max}, not by ΔK_{eff}, and that load order effects are caused by residual stresses *ahead* of the crack tip, not by crack closure *behind* it. It evaluates K_{res}, the residual SIF in any given load event caused by the previous load history, considering the EP material response along the uncracked ligament. To do so, K_{res} values are calculated by integrating over the entire rl the product of the residual stress field by a suitable geometry-dependent weight function, assumed one-dimensional. However, UniGrow supposes that at any load cycle a $K_{res} \leqslant 0$ reduces only its K_{max}. Although somewhat arbitrary and even questionable (see Fig. 1), this hypothesis allows the SIF range ΔK, which is assumed to drive along with K_{max} the FCG process, to become sensitive to the residual stress field ahead of the crack tip. Indeed, without this trick, K_{res} would be cancelled out from the SIF range, as it is in the Willenborg FCG models [31,32]. Moreover, this "K_{res} does not affect K_{min}" hypothesis is considered valid even if the crack surfaces do not contact each other at K_{min}, so do not transfer loads through them.

Anyway, the key issue in the UniGrow model is how to calculate, at each and every load cycle, the residual stress field $\sigma_{res}(x)$ ahead of the crack tip, needed to obtain the resulting K_{res} value from the weight-function integral. Having estimated K_{res}, UniGrow uses Eq. (1) to estimate FCG rates, where A_{ug} and m_{ug} are material parameters:

$$da/dN = A_{ug} \cdot \left[(K_{max} + K_{res})^p \cdot (\Delta K + K_{res})^{1-p} \right]^{m_{ug}} \quad (1)$$

Being a CDM, UniGrow assumes the uncracked ligament consists of several VE or material blocks that behave analogously to tiny εN test specimens ahead of the crack tip, successively breaking them as the crack tip advances. However, instead of using a critical damage model based on some damage accumulation rule to find the variable width of each VE under VAL, it somewhat arbitrarily supposes that their width is not only constant, but a material property ρ^* as well, called the elementary material block size, see Fig. 2. Moreover, instead of estimating the crack tip radius as a function of the CTOD under VAL, such radius is assumed constant and equal to the same material parameter ρ^*. The stress and strain fields ahead of the crack tip are then determined assuming the crack is a sharp notch with a fixed small tip radius ρ^*, from which damage is calculated using εN procedures to find the number of cycles N^* needed to break each material block of width ρ^* [30].

The N^* calculation assumes an opened crack of length a, modeled using the stress concentration factor $K_t = K_t(a, \rho^*)$ of a notch of length a and tip radius ρ^*. A closed crack, on the other hand, is assumed to behave as if it was a circular hole with radius ρ^*, because the crack surfaces are supposed to perfectly contact each other under compressive loads, transmitting the applied forces except in a small circular region just behind the crack tip. Crack surface closure is assumed to happen exactly at $K = 0$, thus any K_{max} or $K_{min} < 0$ is associated with a circular hole with $K_t = 3$, while any K_{max} or $K_{min} > 0$ has $K_t = K_t(a, \rho^*) >> 3$. This way, the UniGrow model can consider the damage contribution of the stress and strain ranges that happen ahead of the crack tip even while the crack is partially closed (because the K_{min} values affect the ΔK range).

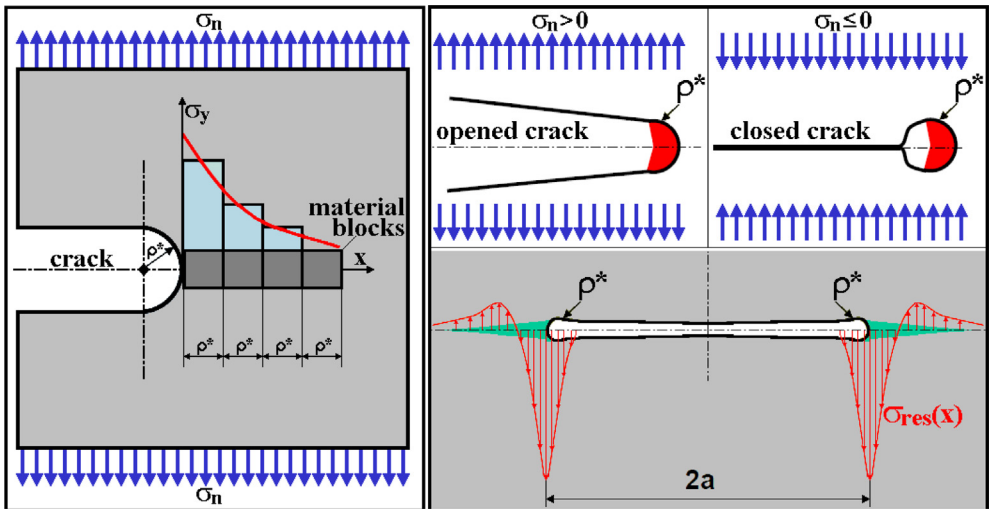

Fig. 2. UniGrow's materials blocks (left), and the assumed fatigue crack configurations when it is closed and opened (right) [2].

Notice that fatigue damage ahead of the crack tip while $K_{min} < K_{op}$ is completely neglected by FCG models based on Elber's idea, which assume no fatigue damage can happen while the crack is not totaly opened. UniGrow considers damage even while the crack is partially or totally closed, but this asset may be questioned because it neglects any possible crack closure contribution. Moreover, UniGrow estimates the stress field ahead of the crack tip using Creager and Paris' linear elastic (LE) solution for a blunt notch, neglecting significant yielding effects near the crack tip. This LE field is used with the cyclic Ramberg-Osgood curve and Neuber's strain concentration rule to calculate the EP stress and strain fields ahead of the crack tip [30]. Damage at each VE is then calculated using the Smith-Watson-Topper (SWT) fatigue damage parameter. But instead of using a damage profile ahead of the crack tip to model FCG using εN procedures, damage is calculated only at the VE adjacent to the crack (modeled as a notch) tip, to obtain its life N^*. Since this material block has width ρ^* (supposed constant), the FCG rate is estimated as $da/dN = \rho^*/N^*$. This hypothesis is used to calibrate the ρ^* parameter from da/dN data measured under the same loading conditions used to calculate the material block life N^*. The ρ^* calibration uses a least-squares method to collapse all da/dN curves of a given material from a set of measured da/dN data and associated εN calculated N^* lives. However, the fact that ρ^* can collapse da/dN curves does not validate the UniGrow model, because other normalization procedures can perform the same task as well, as clearly shown by Kujawski [34]. Such model might be validated if a ρ^* parameter with the ability to robustly collapse da/dN curves could be accurately *predicted* using some physically-based model, but this is not the case, since ρ^* is numerically fitted for that purpose.

After the ρ^* parameter and Eq. (1) are calibrated, fatigue damage simulations under VAL conditions still require a cycle-by-cycle calculation of the residual stress profile ahead of the crack tip to obtain K_{res} after every load event. To decrease computational costs, residual stress fields induced by each loading event are assumed qualitatively similar, and estimated as a scaled version calibrated from the calculated stress at the VE adjacent to the current crack tip (treated as a sharp notch). However, since plasticity induces memory effects, the stress field ahead of the crack tip depends on the current load cycle and also on the residual fields generated by previous load events. UniGrow uses relatively simple empirical "memory rules" to combine the residual stress fields calculated after each load cycle. Such rules basically state that the residual stress at any material block is equal to the minimum stress applied so far in the history at that block, except in the presence of underloads, which tend to erase OL effects and require additional memory rules. Moreover, only the compressive part of the residual stress field is assumed to affect the FCG process.

In summary, UniGrow assumes several simplifying hypotheses, such as: closed crack tips can be modeled as circular holes with a constant radius ρ^*; VE or material blocks that successively break ahead of the crack tip have the same width ρ^*; crack surfaces contact exactly at $K = 0$; notch-tip strains can be estimated by Creager and Paris and Neuber's rule, even under plane strain conditions; residual stresses affect K_{max} but not K_{min}, even when it is positive; residual stress profiles can be assumed similar; the interaction between them can be modeled through very simple memory rules; and finally the residual SIF K_{res} can be assumed as a linear function of the net SIF for each R-level. The use of so many phenomenological hypotheses, although qualitatively coherent with experiments, can quantitatively compromise the accuracy of UniGrow predictions. This issue is hidden by the very high sensitivity of FCG life predictions to ρ^*. Indeed, subtle changes in ρ^* are usually enough to fit experimental data. However, such a post-mortem fitting is only applicable to failure analyses, undermining the robustness of the UniGrow model to predict load interaction effects, since small ρ^* calibration errors can result in very different FCG predictions. In summary, ρ^* probably is not a material property, but instead a highly sensitive curve-fitting parameter, used to compensate for the errors caused by the many simplifications adopted in the UniGrow model.

The CDM proposed in [24–26], on the other hand, uses only physically-based hypotheses, see Fig. 3, so it does not need specific data-fitting parameters. It assumes that (i) fatigue cracks grow by successively breaking small VE located ahead of their tips; (ii) such VE can be treated as tiny εN test specimens fixed along the crack path; (iii) these VE accumulate fatigue damage induced by variable strain ranges, which in the case of CAL increase as the crack tip approaches them; and (iv) the fracture of the VE adjacent to the crack tip occurs because it accumulated the entire damage the material can tolerate. Since constant SIF ranges induce constant FCG rates, the VE widths in such cases can be assumed fixed and equal to the crack increment per cycle $\Delta a \cong da$. Hence, any given VE suffers damage in each and every load cycle, caused by the strain loop range induced by that cycle (beyond the component fatigue limit range), which depends on the distance x between the VE and the fatigue crack tip. The fracture of the VE adjacent to the crack tip occurs when its accumulated damage reaches a critical value, estimated by the linear damage accumulation rule Eq. (2) (or by any other suitable damage accumulation rule):

$$\sum_i (n_i/N_i) = 1 \tag{2}$$

where N_i is the number of cycles that the VE would last if only the ith amplitude cycle acted during its entire life, and n_i is the number of cycles that acted during that event.

The main issue in this CDM is to determine the strain range field, since models for stress/strain fields inside the plastic zones that assume a zero tip radius $\rho = 0$, like the HRR field [35,36], are singular at $x = 0$. This physically inadmissible feature, since no cracks under loads can sustain infinite strains at their crack tips, was originally eliminated by shifting the HRR field origin into the crack by a distance X, inspired by Creager and Paris' idea [37]. For constant SIF range conditions, the sum in Eq. (2) can be approximated by an integral along, say, the reverse or cyclic plastic zone (pz_r), neglecting in a first approximation fatigue damage outside it:

$$\frac{da}{dN} = \int_0^{pz_r} \frac{dx}{N(x+X)} \tag{3}$$

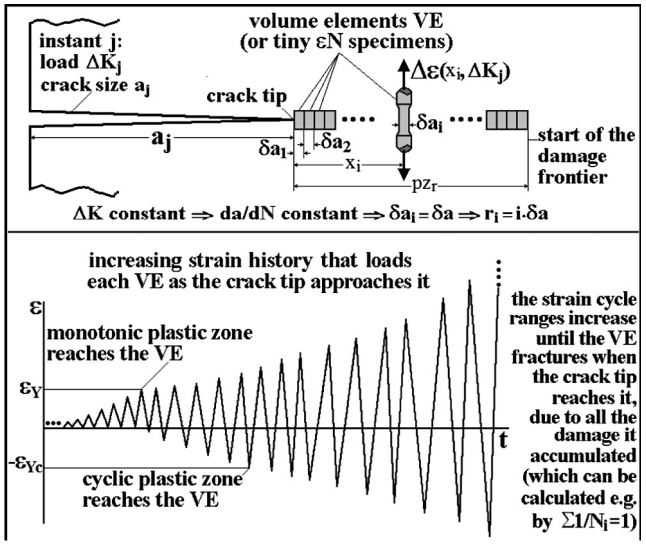

Fig. 3. Schematics of the FCG caused by fracture of a VE at every load cycle [2].

The HRR field origin shift X can be estimated in two ways: (i) assuming $X = \rho/2$, as Creager and Paris did, where ρ is the crack tip radius under K_{max}; or (ii) by first calculating the plastic strain range $\Delta\varepsilon_p(X)$ acting at the crack tip using a suitable strain concentration rule and the crack LE stress concentration factor K_t, describing it as a sharp notch with the same length a, but with a finite tip radius $\rho > 0$. Then, to calculate the cyclic plastic strain range $\Delta\varepsilon_p$ ahead of the crack tip, the modification of the HRR strain field proposed by Schwalbe [28] can be used as in [25]:

$$\Delta\varepsilon_p(x+X) = (2S_{Yc}/E)\cdot[pz_r/(x+X)]^{1/(1+h_c)} \tag{4}$$

where S_{Yc} is the cyclic yield strength of the material, E is its Young's modulus, and h_c is its Ramberg-Osgood strain-hardening exponent.

Since the elastic strain amplitude inside the cyclic plastic zone is neglected in Eq. (4), its associated fatigue life $N(x + X)$ can be estimated from the plastic part of Coffin-Manson's equation as

$$N(r+X) = (1/2)[\Delta\varepsilon_p(x+X)/2\varepsilon_c]^{1/c} \tag{5}$$

where c and ε_c are Coffin-Manson's plastic exponent and coefficient, respectively.

Using half of the crack tip radius to estimate the X displacement of the modified HRR field, and assuming $\rho = CTOD/2$, then

$$X = \frac{\rho}{2} = \frac{CTOD}{4} = \frac{K_{max}^2\cdot(1-2\nu)}{\pi\cdot E\cdot S_{Yc}}\cdot\sqrt{\frac{1}{2(1+h_c)}} \tag{6}$$

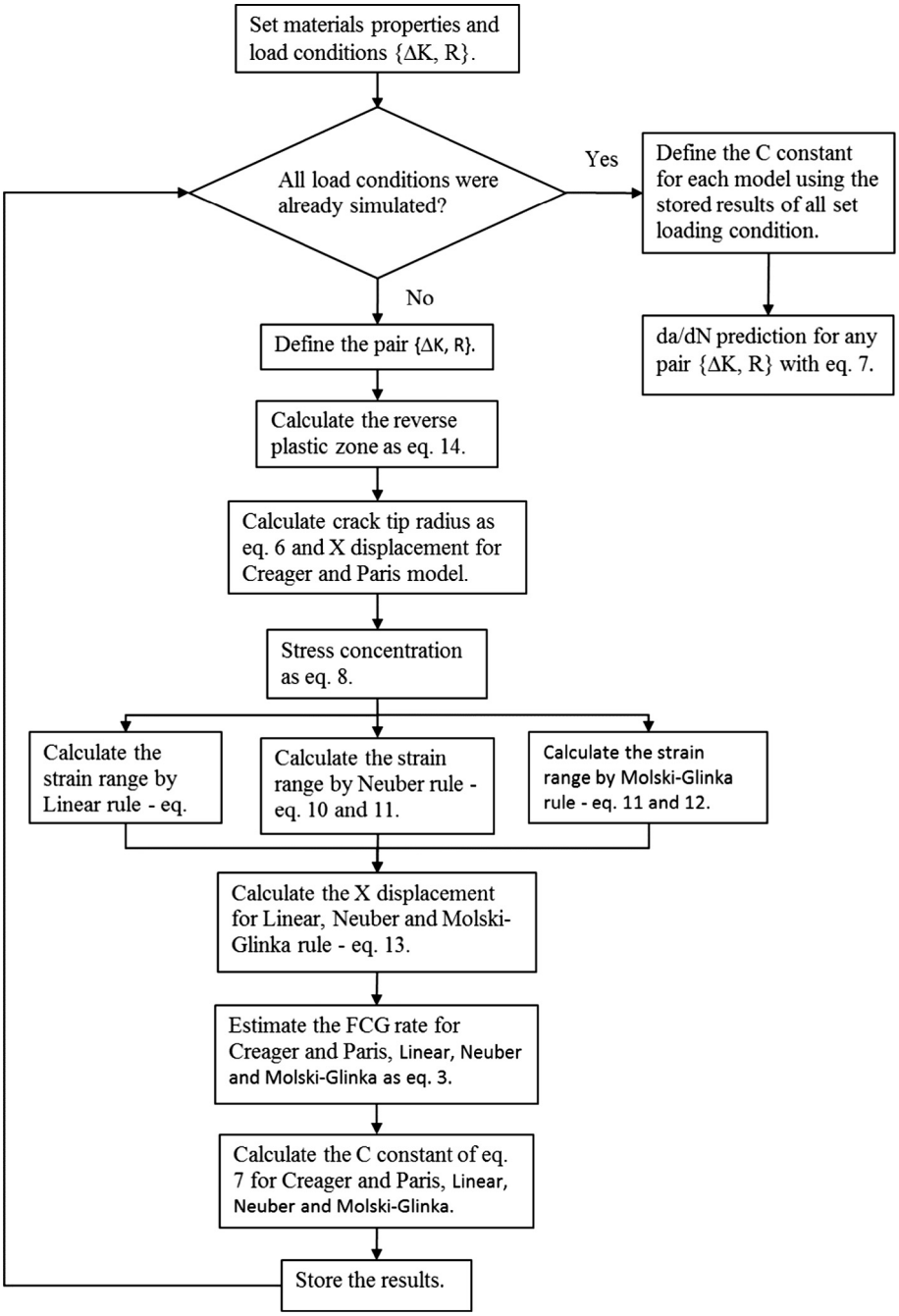

Fig. 4. Flow diagram for critical damage models.

Substituting Eq. (4) into Eq. (5) and then using Eq. (3), it is possible to estimate the FCG rate induced by any {ΔK, R} calculating the constant C in a modified McEvily's rule to simulate all 3 phases of typical $da/dN \times \Delta K$ curves:

$$da/dN = C \cdot (\Delta K - \Delta K_{th})^2 \cdot [K_c/(K_c - K_{\max})] \quad (7)$$

Notice that this step is needed to properly consider the fracture toughness K_c and the FCG threshold ΔK_{th} limits in FCG rates, since in the adopted approach no upper or lower strain bounds are set in Coffin-Manson's equation to model fracture or the fatigue limit, respectively. Another less arbitrary way to estimate the X displacement is to use Creager and Paris' K_t estimation and a suitable strain concentration rule to evaluate the strain range $\Delta\varepsilon_p$ at the crack tip:

$$K_t \cdot \Delta\sigma_n = 2\Delta K/\sqrt{\pi \cdot \rho} \quad (8)$$

Assuming $\rho \cong CTOD/2$, for any given ΔK it is possible to estimate the product $K_t \cdot \Delta\sigma_n$ and then, using the chosen strain concentration rule (Neuber, Molski-Glinka, Linear, or any other), the plastic strain

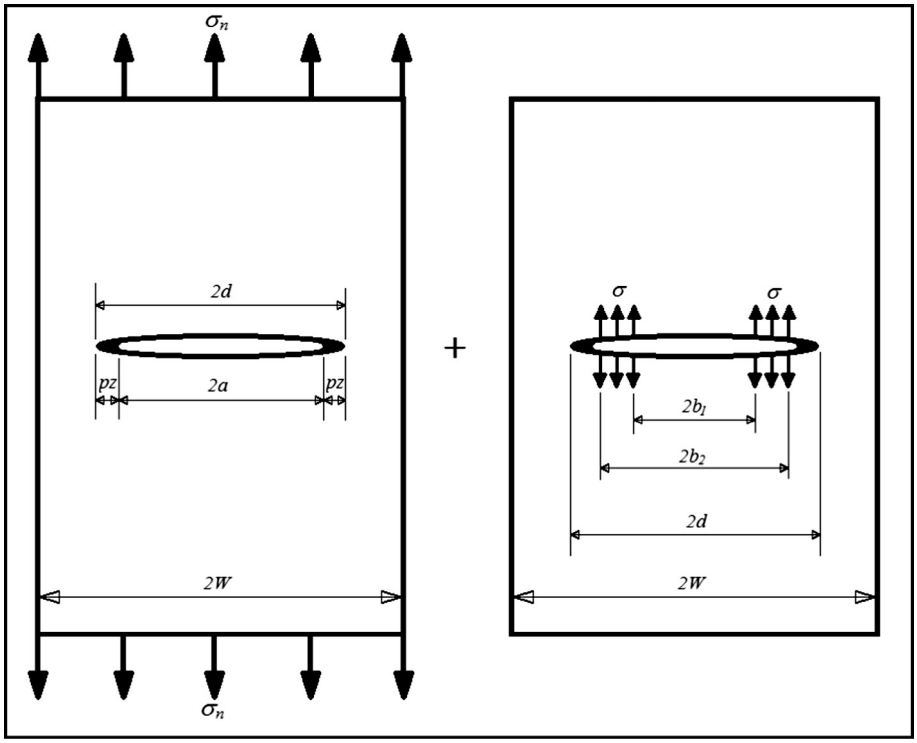

Fig. 5. (a) M(T) specimen with a crack of size $2(a + pz)$ loaded by a remote tensile stress σ_n; and (b) M(T) specimen with a crack of size $2(a + pz)$ loaded by symmetrical distributed stresses σ over the two segments near the crack tips [6].

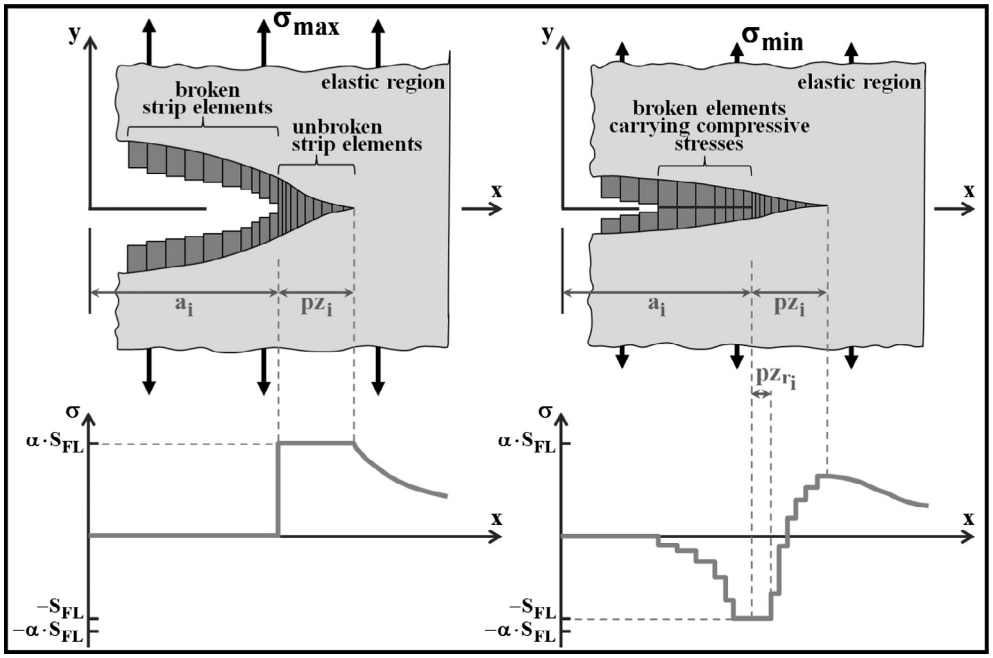

Fig. 6. Crack surface displacements and stress distribution along the crack line [6].

range can be estimated at the crack tip. The $\Delta\varepsilon_p$ estimate by the Linear rule is obtained using Eq. (9), by Neuber using Eqs. (10) and (11), and by Molski-Glinka using Eqs. (11) and (12):

$$\Delta\varepsilon_p(X) = \frac{K_t \cdot \Delta\sigma_n}{E} = \frac{2 \cdot \Delta K}{E \cdot \sqrt{\pi \cdot CTOD/2}} \tag{9}$$

$$\Delta\sigma(X) \cdot \Delta\varepsilon_p(X) = \frac{(K_t \cdot \Delta\sigma_n)^2}{E} = \frac{8 \cdot \Delta K^2}{E \cdot \pi \cdot CTOD} \tag{10}$$

$$\Delta\varepsilon_p(X) = 2 \cdot (\Delta\sigma(X)/2H_c)^{1/h_c} \tag{11}$$

$$\frac{2\Delta K^2}{E \cdot \pi \cdot CTOD} = \frac{\Delta\sigma(X)^2}{4E} + \frac{\Delta\sigma(X)}{h_c + 1} \cdot \left(\frac{\Delta\sigma(X)}{2H_c}\right)^{1/h_c} \tag{12}$$

After estimating $\Delta\varepsilon_p$ at the crack tip, the X displacement of the HRR field can be found from Eq. (13) and the cyclic plastic zone, as shown in Eq. (14):

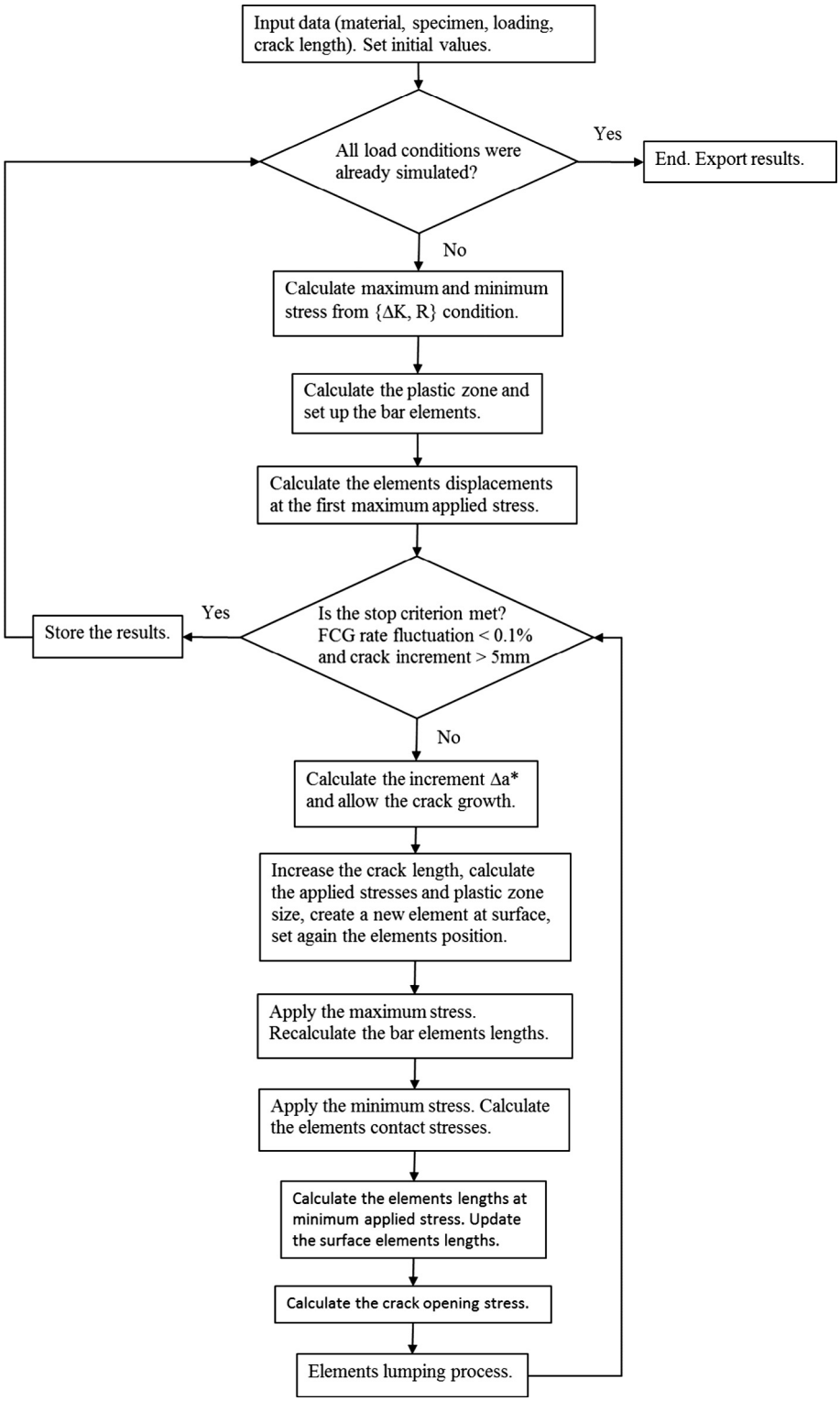

Fig. 7. Flow diagram for the strip-yield model.

$$X = pz_r \cdot \left[\Delta\varepsilon_p(X) \cdot E/(2S_{Yc})\right]^{-(1+h_c)} \tag{13}$$

$$pz_r = (1-2\nu)^2/[4\pi(1+h_c)] \cdot (\Delta K/S_{Yc})^2 \tag{14}$$

Fig. 4 shows the flow diagram of the calculation process for these critical damage models. It can be concluded that the entire $da/dN \times \Delta K$ curve can be estimated using only well-defined material properties, without the need for any specific data-fitting parameter. The presented equations apply only to constant SIF range conditions, so they describe the simplest formulation of this CDM, but this model can be further developed to describe FCG under VAL as well, see [26].

3. Strip-yield models

SYMs numerically estimate the crack opening SIF K_{op} needed to find ΔK_{eff} using the classic Dugdale-Barenblatt's model [38,39], modified to leave plastically deformed material around the faces of the advancing fatigue crack [5–9]. Newman's original SYM [6] is based on Elber's PICC idea and was developed for a finite plate with a central crack loaded by a uniform tensile stress σ_n. The pz sizes and surface displacements are obtained by the superposition of two LE problems: (i) a cracked plate loaded by a remote uniform nominal tensile stress σ_n (see Fig. 5a), and (ii) by a uniform distributed stress σ applied over crack surface segments (see Fig. 5b).

Fig. 6 shows the crack surface displacements and the stress distributions around the crack tip at the maximum σ_{max} and minimum σ_{min} applied stresses. It is composed of three regions: (1) a linear elastic region containing a fictitious crack of half-length $a + pz$; (2) a plastic region of length pz and (3) a residual plastic deformation region along the crack surface. The plastic zone is discretized in a series of rigid-perfectly plastic 1D bar elements, which are assumed to yield at the flow strength of the material, $S_F = (S_Y + S_U)/2$, to somehow account for the otherwise neglected strain-hardening effects. These elements are either intact at the plastic zone or broken at the crack wake, storing the residual plastic deformations. If they are in contact, the broken bar elements can carry compressive stresses, therefore they can yield in compression when their stresses reach $-S_F$. The elements along the crack face that are not in contact do not affect the crack surface displacements, or carry stresses.

This SYM uses a constraint factor α to increase the tensile flow stress S_F in the unbroken elements along the plastic zone during loading. This is done to consider the effects of the actually 3D stresses around the crack tip, caused by plastic restrictions when the plate is thick and cannot be assumed to work under pl-σ. So, this constraint factor should vary from $\alpha = 1$ for plane-stress to up to $\alpha = 1/(1-2\nu) \cong 3$ for plane-strain limit conditions, where ν is Poisson's coefficient (albeit in practice α is often used as a data fitting parameter when using this SYM). Since there is no crack-tip singularity when the crack closes, this constraint factor is not used to modify the compressive yield stress during unloading, assuming the conditions around the crack tip tend to remain uniaxial.

The coordinate system shown in Fig. 6 is fixed and its origin lies at the center of the central crack, whose length is $2a$. Due to symmetry, only one quarter of the plate needs to be analyzed. Eq. (16) governs the system response by requiring compatibility between the LE part of the cracked plate and all bar elements. When the wake elements' length L_j is larger than their displacement V_j under σ_{min}, they come into contact and induce a stress σ_j needed to force $V_j = L_j$. The influence functions $f(x_i)$ and $g(x_i, x_j)$ used in Eq. (16) are related to the plate geometry and its width correction, as expressed in Eqs. (17)–(19).

$$V_i = \sigma_n \cdot f(x_i) - \sum_{j=1}^{n} \sigma_j \cdot g(x_i, x_j) \tag{16}$$

$$f(x_i) = [2(1-\eta^2)/E] \cdot \sqrt{(d^2 - x_i^2)\sec(\pi d/2W)} \tag{17}$$

$$g(x_i, x_j) = G(x_i, x_j) + G(-x_i, x_j) \tag{18}$$

$$G(x_i,x_j) = \frac{2(1-\eta^2)}{E}\left\{(b_2 - x_i)\cdot\cosh^{-1}\left(\frac{d^2 - b_2 x_i}{d|b_2 - x_i|}\right) - (b_1 - x_i)\cdot\cosh^{-1}\left(\frac{d^2 - b_1 x_i}{d|b_1 - x_i|}\right) + \right.$$
$$\left. + \sqrt{d^2 - x_i^2}\cdot\left[\sin^{-1}(b_2/d) - \sin^{-1}(b_1/d)\right]\cdot\left[\frac{\sin^{-1}B_2 - \sin^{-1}B_1}{\sin^{-1}(b_2/d) - \sin^{-1}(b_1/d)}\right]\cdot\sqrt{\sec\left(\frac{\pi d}{2W}\right)}\right\} \tag{19}$$

Notice that $\eta = 0$ for plane stress and $\eta = \nu$ for plane strain, and that B_1 and B_2 are calculated from Eq. (20), b_1 and b_2 from Eqs. (21) and (22), and the plastic zone pz from Eq. (23) and (24).

$$B_k = \sin(\pi b_k/2W)/\sin(\pi d/2W) \tag{20}$$

$$b_1 = x_j - w_j \tag{21}$$

$$b_2 = x_j + w_j \tag{22}$$

$$pz = a\left\{(2W/\pi a)\cdot\sin^{-1}\{\sin(\pi a/2W)\cdot\sec[\pi\sigma_{max}f/(2\alpha S_F)]\} - 1\right\} \tag{23}$$

$$f = 1 + 0.22(a/W)^2 \tag{24}$$

In Fig. 6, pz is divided into 20 bar elements with variable widths $2w_i/pz = 0.005, 0.005, 0.005, 0.005, 0.01, 0.01, 0.02, 0.02, 0.03, 0.03, 0.045, 0.045, 0.06, 0.06, 0.075, 0.075, 0.1, 0.1, 0.15, 0.15$. The smallest element $n = 1$ is the nearest of the crack tip, at $x = a$. After calculating the pz size induced by the current cycle peak stress σ_{max}, the lengths of the bar elements inside the plastic zone are calculated from:

$$L_i = V_i = \sigma_{max} \cdot f(x_i) - \sum_{j=1}^{20} \alpha \cdot S_F \cdot g(x_i, x_j) \tag{25}$$

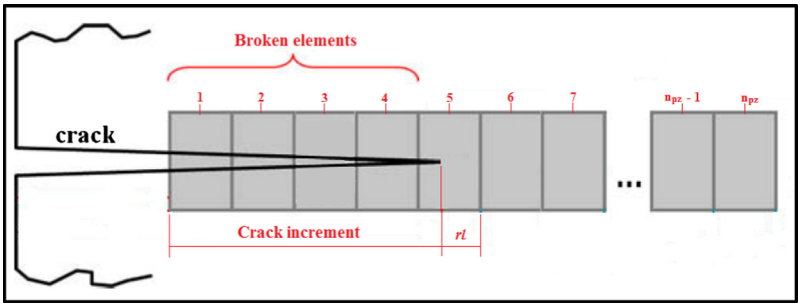

Fig. 8. Schematic of the rupture of elements VE_1 through VE_4 and part of VE_5.

When the plate is unloaded down to σ_{min} (Fig. 5b), the bar elements inside *pz* unload until some of them near the crack tip start to yield in compression, when they try to reach a stress $\sigma_j \leq -S_F$. The broken elements located inside the plastic wake formed along the crack surfaces, which store residual deformations, may come into contact and carry compressive stresses as well. Some of these

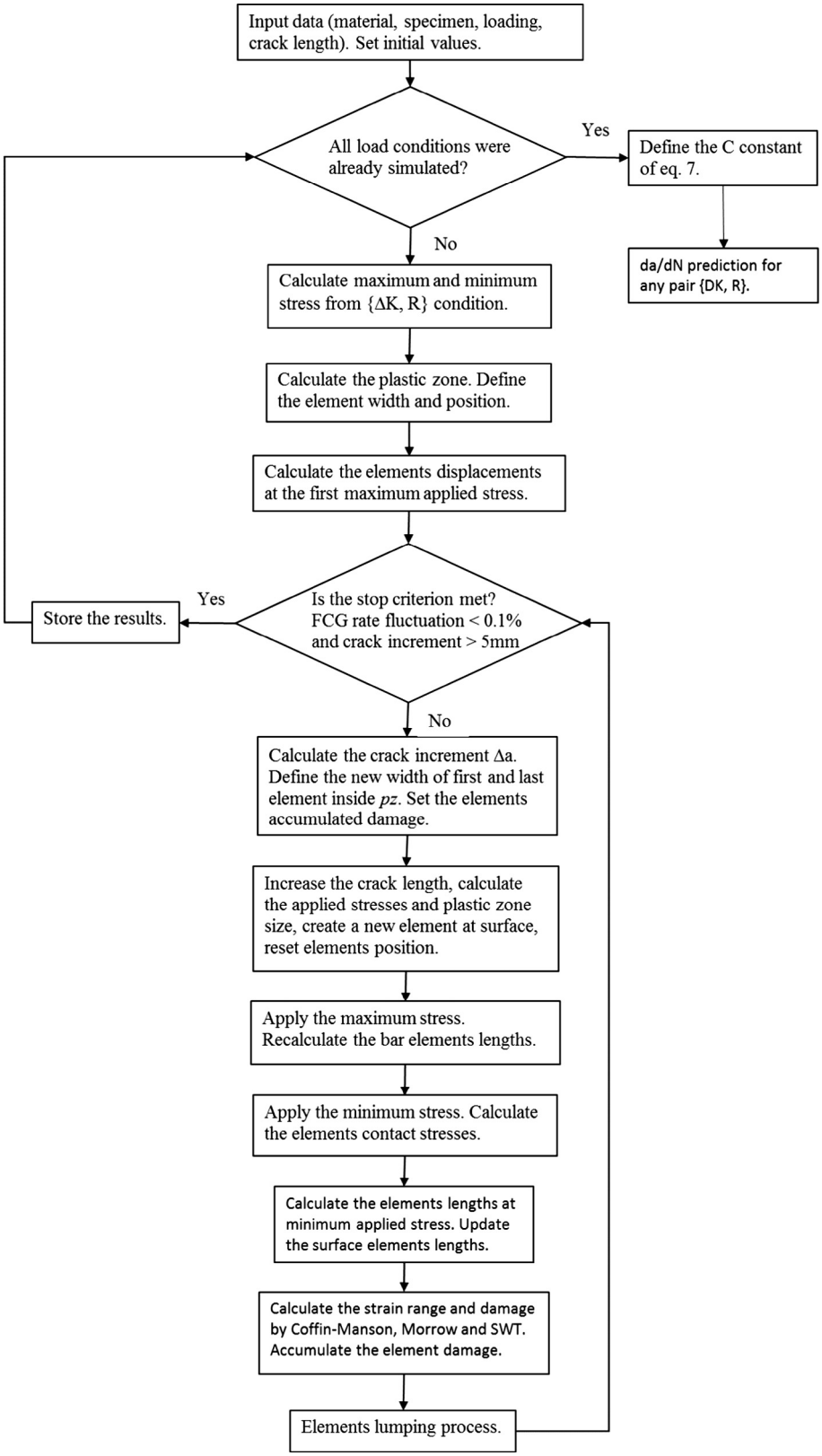

Fig. 9. Flow diagram of the SY-CDM.

Table 1
Material properties [25] and C values obtained by several strain concentration rules.

Material	S_Y (MPa)	S_U (MPa)	K_c (MPa$\sqrt{m}$)	ΔK_{th} (MPa$\sqrt{m}$)		C (for ΔK in MPa$\sqrt{m}$)			
				$R = 0.1$	$R = 0.7$	C&P	Linear	Neuber	M&G
7075-T6	498	576	25.4	3.4	2.9	8.23×10^{-9}	8.84×10^{-9}	2.22×10^{-9}	1.77×10^{-8}
1020	285	491	277	11.6	7.5	2.73×10^{-10}	2.42×10^{-10}	1.38×10^{-9}	1.03×10^{-9}

Table 2
Properties and parameters from the NASGRO 4.02 database [41].

Material	S_Y (MPa)	S_U (MPa)	K_c (MPa$\sqrt{mm}$)	ΔK_1 (MPa$\sqrt{mm}$)	C (for ΔK in MPa$\sqrt{mm}$)	n	p	q	C_{th}	α
7075-T6(M7HA03AB1)	461.9	524	729.7	26.06	9.686×10^{-12}	3	0.5	1	2.5	2
1015-1026(C1BB11AB1)	262	399.9	1737	116.4	1.515×10^{-14}	3.7	0.5	0.5	1.5	2.5

Table 3
Constant C for modified CDMs obtained from SYM–calculated cyclic strain fields.

εN equation	C (for ΔK in MPa$\sqrt{m}$)	
	7075-T6	1020 steel
Coffin-Manson	1.73×10^{-9}	2.64×10^{-9}
Morrow EP	1.45×10^{-7}	1.57×10^{-8}
SWT	1.66×10^{-8}	5.10×10^{-9}

elements may also yield in compression, if they try to reach $\sigma_j \leq -S_F$. The stresses σ_j at each of the n elements in the plastic zone and along the crack surface are calculated by

$$\sum_{j=1}^{n} \sigma_j \cdot g(x_i, x_j) = \sigma_{\min} \cdot f(x_i) - L_i \tag{26}$$

This system of equations is solved by Gauss-Seidel's iterative method with added constraints. The constraints are related to the yield behavior in tension and compression for the bar elements inside the pz, see Eqs. (27) and (28), and to element separation and compressive yielding for the elements along the plastic wake that envelops the crack surfaces, see Eqs. (29) and (30).

$$For\ x_j > a, if\ \sigma_j > \alpha \cdot S_F\ set\ \sigma_j = \alpha \cdot S_F \tag{27}$$

$$For\ x_j > a,\ if\ \sigma_j < -S_F\ set\ \sigma_j = -S_F \tag{28}$$

$$For\ x_j \leqslant a,\ if\ \sigma_j > 0\ set\ \sigma_j = 0 \tag{29}$$

$$For\ x_j \leqslant a,\ if\ \sigma_j < -S_F\ set\ \sigma_j = -S_F \tag{30}$$

From the stresses in the elements at the minimum load, their plastic residual deformations can be calculated using Eq. (31). For the elements not in contact, it follows that σ_i=0 and L_i<V_i.

$$L_i = V_i = \sigma_{\min} \cdot f(x_i) - \sum_{j=1}^{n} \sigma_j \cdot g(x_i, x_j) \tag{31}$$

The stress σ_{op} that completely opens the crack surfaces is calculated from Eqs. (32) and (33) with $k = 1$ or 2 [40]. In these equations, a_w is the sum of the initial crack length and of all element widths at the crack surface, but the width for the element n is replaced by the largest crack growth increment during the generation of Δa^*, not by the entire increment over which the opening stress is held constant.

$$\sigma_{op} = \sigma_{\min} - \sum_{j=21}^{n} (2\sigma_j/\pi)[\sin^{-1} B_2 - \sin^{-1} B_1] \tag{32}$$

$$B_k = \sin(\pi b_k/2W)/sin(\pi a_w/2W) \tag{33}$$

σ_{op} is kept constant during a small arbitrary crack increment Δa^*, to save computational cost. At the maximum load, Δa^* is calculated from Eq. (34), where $R_x = R = \sigma_{\min}/\sigma_{\max}$ if $R > 0$ and $R_x = 0$ if $R \leq 0$. In the original FASTRAN code, the crack increment is assumed to be $\Delta a^* = 0.05 \cdot pz$, and Eq. (34) is used to improve the opening stress calculations for higher stress ratios [40].

$$\Delta a^* = 0.2(pz/4) \cdot (1 - R_x)^2 \tag{34}$$

The number of load cycles ΔN needed to grow the crack by this Δa^* increment is calculated by the NASGRO rule, Eq. (35) [41], in which C_n, m, p and q are data fitting parameters, K_c is the fracture toughness, and the threshold ΔK_{th} can be estimated using Eqs. (36) and (37). $\Delta K_1{}^*$ is given by Eq. (38), A_0 by Eq. (39), ΔK_1 is the threshold measured at high R when the crack is closure-free, C_{th} is still another empirical data-fitting constant with different values for positive or negative (superscript p or n) values of R, and a_0 is an "intrinsic crack size" (assumed fixed, $a_0 = 0.0381$ mm). ΔK_1 is also called the intrinsic threshold by ΔK_{eff} supporters, or the threshold of the maximum by the Unified Approach followers, who say that ΔK and $K_{\max}$ are the true fatigue crack driving forces [42].

$$da/dN = C_n(\Delta K_{eff})^m \cdot (1 - \Delta K_{th}/\Delta K)^p/(1 - K_{\max}/K_c)^q \tag{35}$$

$$\Delta K_{th} = \Delta K_1^* \left[(1 - R)/(1 - K_{op}/K_{\max})\right]^{(1+R \cdot C_{th}^p)} / (1 - A_0)^{(1-R)C_{th}^p}, \quad R \geqslant 0 \tag{36}$$

$$\Delta K_{th} = \Delta K_1^* \left[(1 - R)/(1 - K_{op}/K_{\max})\right]^{(1+R \cdot C_{th}^p)} / (1 - A_0)^{(C_{th}^p - R \cdot C_{th}^n)}, \ R < 0 \tag{37}$$

$$\Delta K_1^* = \Delta K_1 [a/(a + a_0)]^{0.5} \tag{38}$$

$$A_0 = (0.825 - 0.34\alpha + 0.05\alpha^2)[\cos(\pi\sigma_{\max}/2S_F)]^{1/\alpha} \tag{39}$$

Table 4
Measured Coffin-Manson properties (notice that εN and da/dN coupons were machined from the same lot of each material, to guarantee the consistency of the measured data).

Material	E (GPa)	σ_c (MPa)	b	ε_c	c
7075-T6	72	709	−0.056	0.12	−0.75
1020	205	815	−0.114	0.25	−0.54

To keep the number of elements reasonable, say less than 40, a lumping process along the plastic wake is used to join the bar elements, combining adjacent elements i and $i+1$ to form a single element when

$$2(w_i + w_{i+1}) \leqslant a - x_{i+1} + \Delta a^* \tag{40}$$

It follows that the elements near the crack tip are not as likely to be lumped together as those that are away from the tip. In the lumping process, the width of the lumped element is the sum of the widths of the two adjacent elements, while its length is the weighted average of the two, namely

$$L = (L_i w_i + L_{i+1} w_{i+1})/(w_i + w_{i+1}) \tag{41}$$

Fig. 7 shows the flow diagram for the implemented algorithm. The stopping criterion was defined here with the objective to find the stabilized FCG rate at a constant SIF range simulation.

4. The combined Strip-Yield critical damage model

To compare the SYMs and CDMs performance, proper calculation procedures are implemented in a code based on the original Newman formulation [6,40]. This inbred code includes as well the NASGRO FCG rule [41], to use the material properties listed in it. The SYM code validation is performed by comparing its crack opening stress predictions for several load combinations under plane stress and plane strain conditions with results reported by Newman [40]. The combined strip-yield critical-damage model (SY-CDM) proposed here estimates the crack growth increments in a cycle-by-cycle basis through a gradual damage accumulation process, considering possible crack closure effects on the cyclic strain field ahead of the crack tip. So, it combines Newman's strip-yield ideas [6] with the cyclic damage accumulation routines developed by Castro et al. [26].

This SY-CDM also divides the monotonic plastic zone pz into small bar elements, analogous to tiny εN specimens. However, as the crack increments are directly calculated from the damage accumulated by such elements as the crack tip approaches them, the number of elements along pz must be larger than in the SYM to improve the calculation accuracy. Under fixed $\{\Delta K, R\}$ loading conditions that induce constant da/dN rates, the element width can be assumed constant too. So, the width of the small bar elements could be arbitrarily chosen, say $2w = 1 \times 10^{-7}$ m. However, to maintain accuracy even when pz is very small, at least 150 bar elements are used ahead of the crack tip. Moreover, to avoid too many elements at high FCG growth rates, their number is limited to 550. As in the original SYM, the first element inside the plastic zone is called element one, but the total number of plastic zone elements varies from 150 to 550.

Crack increments do not necessarily have the width of the VE as assumed in [25], allowing the model to deal with VAL or even with rate transient behavior at the initial simulation phase due to variations of the crack opening load. Like in the SYM, the elements broken as the crack advances are kept along the crack surfaces, and used to consider crack opening stress effects in the cyclic strain field ahead of the crack tip, which can affect the plastic displacement of the unbroken elements inside the plastic zone. Therefore,

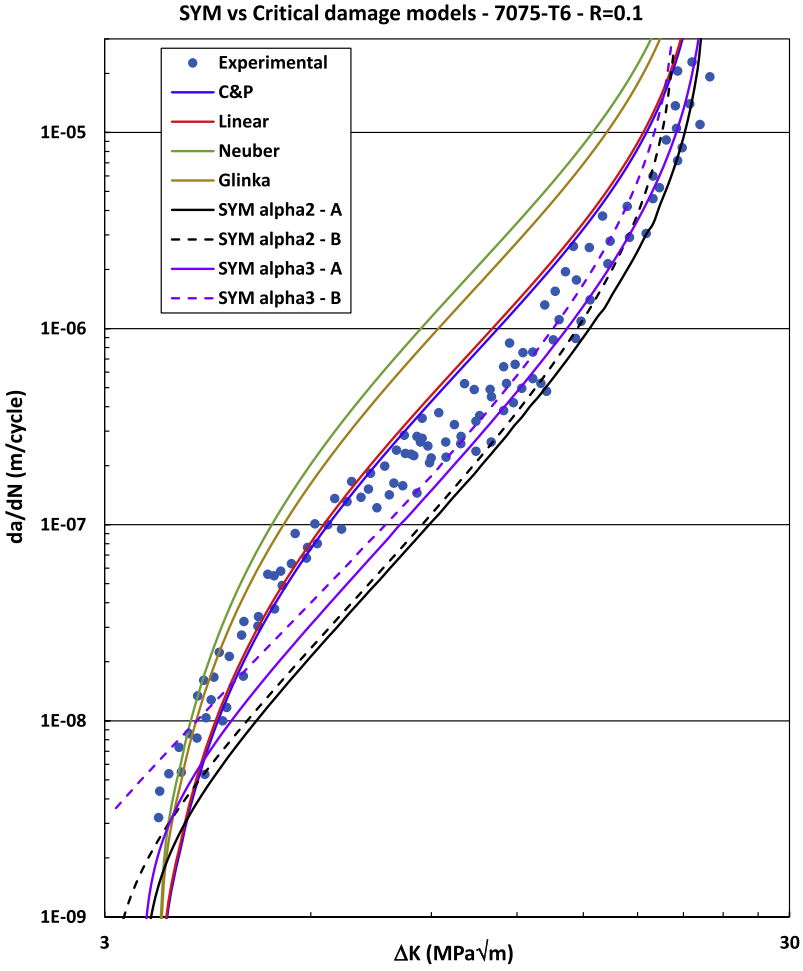

Fig. 10. SYM and original CDM estimates for the FCG curve of the 7075-T6 Al alloy at $R = 0.1$.

although not considered in this work, which deals only with simulations of $da/dN \times \Delta K$ curves measured under constant SIF range conditions, this CDM is versatile and can deal with VAL as well, following ideas outlined in [26].

The SYM procedures calculate peak and residual plastic *displacements* at each bar element, as previously described, so it is necessary to adapt them to generate the strain field needed by this new SY-CDM. For that purpose, it is necessary to transform the cyclic displacements of the elements inside the plastic zone into cyclic strains. This is done by using a solution proposed by Rice [43] to estimate the strain field based on CTOD variations, properly modified to consider the calculated displacements of the various elements through

$$\Delta\varepsilon_y = \log[(2L_{\max}(i) + x_{ct}(i))/(2L_{\min}(i) + x_{ct}(i))] \quad (42)$$

The displacements $L_{\max}$ and $L_{\min}$ of the ith element inside the pz are calculated at the maximum and minimum applied stresses. The positions of the elements starting from the crack tip, $x_{ct}(i)$, are located at the center of each element. The strain range $\Delta\varepsilon_y$ that acts at each element center can be correlated with the number of cycles $N(i)$ that would be required to break that element if that range was kept constant, calculated from the plastic part of Coffin-Manson's rule through Eq. (43), or from Morrow's elastoplastic rule through Eq. (44), or else from SWT's rule through Eq. (45):

$$N(i) = (1/2)(\Delta\varepsilon_y(i)/2\varepsilon_c)^{1/c} \quad (43)$$

$$N(i) = (1/2)\left[(\Delta\varepsilon_y(i)/2\varepsilon_c)(1 - \sigma_m/\sigma_c)^{-c/b}\right]^{1/c} \quad (44)$$

$$N(i) = (1/2)(\sigma_{\max}(i) \cdot \Delta\varepsilon(i)/2\sigma_c\varepsilon_c)^{1/(b+c)} \quad (45)$$

Notice that only the plastic part of the strain range can be considered by this SY-CDM, because strain ranges estimated from the SYM displacements are obtained assuming rigid-perfectly-plastic bar elements, neglecting elastic components. The total damage accumulated by each element can be evaluated by Palmgren-Miner's rule, Eq. (2), or else by any other damage accumulation rule. The stresses σ_m and $\sigma_{\max}$ from Eqs. (44) and (45) are calculated using the maximum ($\sigma_{\max} = \alpha.S_F$) and minimum ($\sigma_{\min} = -S_F$ by Eq. (28) inside the pz_r) stresses that act in each element.

Since this SY-CDM calculates fatigue damage at the central position of each VE, it needs to find the residual ligament rl of the element where the crack tip stops after each load cycle. Then, the model generates a new element with width rl located at the new crack tip (element one), and finds its central position and the fatigue damage associated with it. For the simplest particular case, when the accumulated damage $D(i)$ at the center of the partially broken element i reaches exactly its critical value, its residual ligament becomes half its width (i.e. half of the element would break due to an accumulated damage beyond the spatial average $D(i)$, while the other half would become the residual ligament). To keep the sum of the widths of all elements equal to the pz size, the difference rl is added to the last element n_{pz} located at the pz frontier.

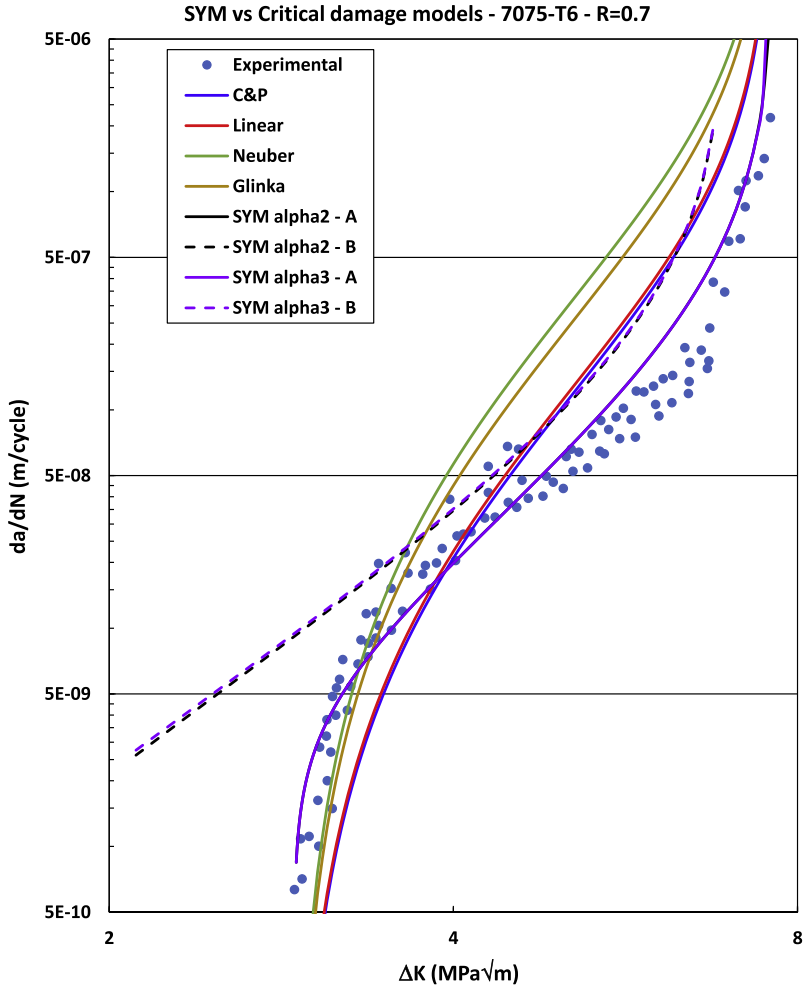

Fig. 11. SYM and original CDM estimates for the FCG curve of the 7075-T6 Al alloy at $R = 0.7$.

As a result, in this model only two bar elements have variable width, the first and the last one. The central position of the new first element is then in the middle of the residual ligament of the partially broken one, and the accumulated damage associated with it is calculated by linear interpolation.

Fig. 8 illustrates the VE distribution and a partially broken bar element after a load cycle, which started with the crack tip located at the VE_1 frontier, and ended with the crack tip located inside (say) VE_5. The estimated crack increment causes the residual ligament of that partially broken VE to become either (i) $rl = w_i$ if $D(5) = 1$, (ii) $rl > w_i$ if $D(5) < 1$, or (iii) $rl < w_i$ if $D(5) > 1$, assuming 1 as the critical value according to Miner's rule. This way, for any $\{\Delta K, R\}$ loading condition, this CDM calculates the corresponding crack growth rate through the fatigue damage accumulated by the cyclic plastic strain history ahead of the crack tip, *considering* possible crack closure effects on the cyclic strain field. Moreover, notice that it is relatively easy to extend this simple calculation scheme to deal with VAL, since the last (and first) element can have a variable width in time. The calculation procedure of this combined SY-CDM is described in Fig. 9.

Since Eq. (7) reproduces the sigmoidal shape of $da/dN \times \Delta K$ curves, and since its only adjustable constant C can be directly calculated for any $\{\Delta K, R\}$ combination from the εN properties of the material, the CDM used here in fact does not have any data-fitting parameter (whereas NASGRO's FCG rule used by the SYM needs 4 of them). Besides, even though McEvily's FCG rule used by the CDM, namely $da/dN = C\cdot(\Delta K - \Delta K_{th})^m\cdot[K_c/(K_c - K_{max})]$, uses a fixed exponent $m = 2$ to model the ΔK effect on da/dN, assuming it is material-independent, it could be modified using a variable m easily calculated as well from the εN properties of the material, by finding several FCG rates associated with various $\{\Delta K, R\}$ loading combinations. This can be done using either Eq. (3) to displace the HRR field according to some strain concentration rule as in the original CDMs [24–26], or the non-singular strain fields generated by SYM procedures as discussed above. Finally, a major benefit of all CDMs used in this work must be emphasized: if they can reasonably estimate FCG rates of a given material, they do so using *only* its εN, FCG threshold, and fracture toughness properties, without needing any adjustable FCG data-fitting parameters. Therefore, these simple and sound models can indeed be called *predictive*, since they do not need or use actual FCG data points to estimate da/dN rates. The results presented next support this claim.

5. Results and discussions

The SYM, the CDM and the new combined SY-CDM approaches described above are used to simulate $da/dN \times \Delta K$ data measured at $R = 0.1$ and $R = 0.7$ for two materials, a 7075-T6 aluminum alloy and a 1020 low carbon steel, using C(T) specimens with width 50mm and thickness 10mm and following standard ASTM E647 procedures, as described elsewhere [25]. Table 1 lists these material properties and the C values used by the CDMs to simulate the measured $da/dN \times \Delta K$ curves by Eq. (7). Recall that these C values are *calculated* from the εN-computed damage accumulated by

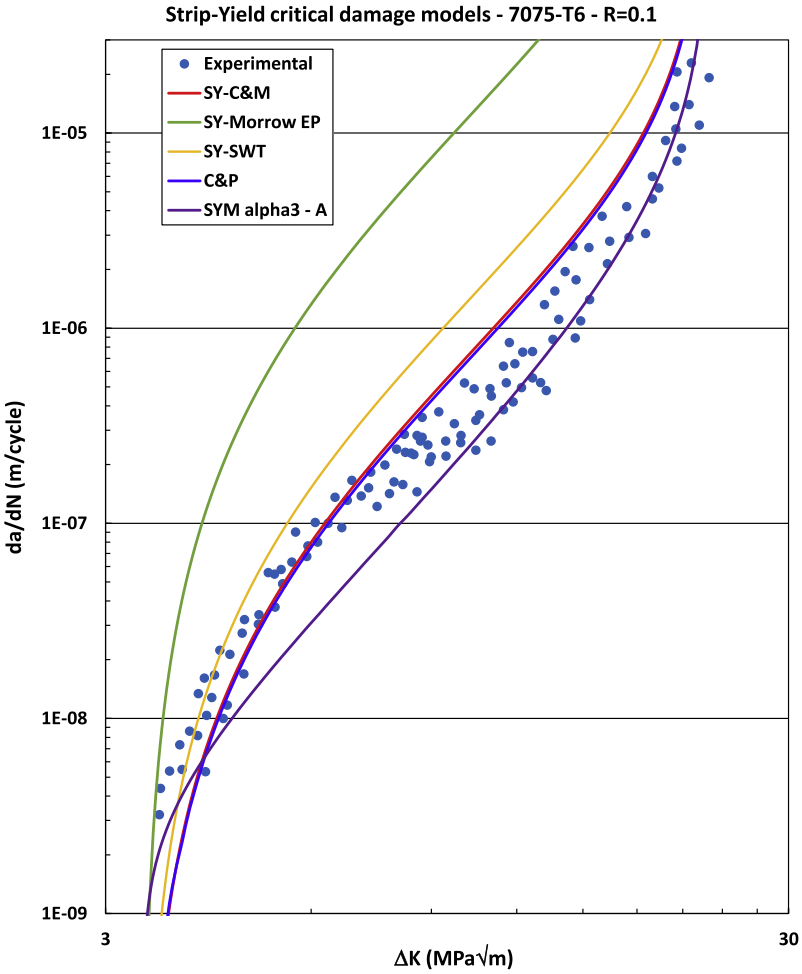

Fig. 12. SYM and SY-CDM FCG estimates for the 7075-T6 Al alloy at $R = 0.1$.

the cyclic strain fields ahead of the crack tip by the HRR field, displaced according to a chosen strain concentration rule to eliminate the crack tip singularity. So, they are *not* obtained by fitting the measured $da/dN \times \Delta K$ data points.

Table 2 gives the parameters and the constraint factor from NASGRO's database for materials similar to the ones tested here. These parameters were used in the SYM calculations to simulate the measured $da/dN \times \Delta K$ curves. Table 3 lists the constants C from Eq. (7), calculated for the two materials by the SY-CDMs using the cyclic strain field generated by SYM bar elements and several εN rules. Table 4 lists the εN properties of the tested materials.

Figs. 10 and 11 depict the $da/dN \times \Delta K$ data points measured in standard tests, as well as the FCG curves predicted by the CDMs [13,25] and by the SYMs for the 7075-T6 Al alloy tested under $R = 0.1$ and $R = 0.7$, respectively. To evaluate possible effects of the tested specimen thickness, the SYM estimates for the FCG curves are obtained using two constraint factors, $\alpha = 2$ and $\alpha = 3$. Moreover, since the Al 7075-T6 properties extracted from the NASGRO database are not identical to those measured in [25], to be fair the SYM simulations are numerically generated under two different conditions, called A and B. SYM–A uses Eq. (35), parameters from Table 2, and measured FCG rate thresholds $\Delta K_{th}(R)$ and toughness K_C listed in Table 1, since these values are also used by the CDM estimates. SYM–B simulations, on the other hand, use only NASGRO recommended parameters listed in Table 2, and apply them in Eqs. (36), (38), and (39) to estimate the corresponding $\Delta K_{th}(R)$ value from Eq. (35). This sensible exercise indicates that SYM estimations are quite sensitive to the FCG threshold and the fracture toughness values used in the simulations. This is not a surprise, since the use of estimated fatigue properties is a risky procedure, to say the least [44].

Recall that the $da/dN \times \Delta K$ curves estimated by the original CDMs are based on the progressive accumulation of εN damage on VEs distributed ahead of the crack tip, which is assumed caused by cyclic HRR fields properly displaced into the crack to eliminate their (non-physical) singularity. As shown in Figs. 10 and 11, the FCG curves generated by the original CDMs that shift the HRR field origin using Creager and Paris (C&P) or the Linear strain concentration rule are similar, and they yield better results than the FCG curves estimated using the Neuber or the Molski-Glinka (M&G) strain concentration rules. Indeed, Neuber and M&G estimate too conservative FCG rates, with the latter being less conservative than the former, as expected. In fact, the better performance obtained from the CDM + Linear rule predictions could be expected as well from fatigue cracks that grow under predominantly plane strain (pl-ε) conditions [2]. The CDM + C&P predictions with $R = 0.1$, which are essentially identical to the CDM + Linear ones, are slightly higher than the da/dN data trend along almost the entire ΔK range, and do reproduce quite well the measured $da/dN \times \Delta K$ data points, which covered all three phases of the FCG process.

On the other hand, CDM procedures estimated lower da/dN rates at low ΔK and higher rates at high ΔK ranges than the measured data at $R = 0.7$, but the differences were relatively small. This quite reasonable performance certainly is not a coincidence, since

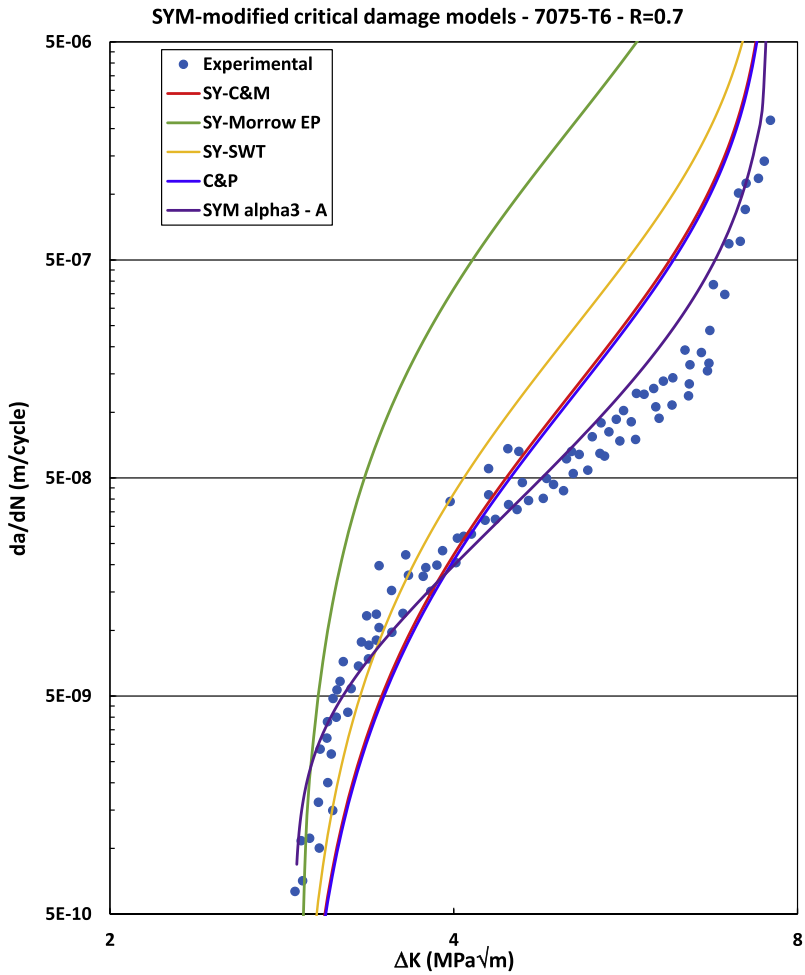

Fig. 13. SYM and SY-CDM FCG estimates for the 7075-T6 Al alloy at $R = 0.7$.

these *predictions* are based only on measured εN properties and use no additional adjustable data-fitting parameters. In fact, when compared to equally reasonable SYM estimates based on ΔK_{eff} concepts, but that need a FCG rule with 4 adjustable parameters, not to mention a constraint factor α that in practice is frequently used as a 5th data-fitting parameter, the CDM performance could be even qualified as quite impressive.

The SYM–A FCG rate estimates for the 7075-T6 Al alloy, made using its measured threshold $\Delta K_{th}(R)$ and fracture toughness K_c values, are much better than the SYM–B ones, made using NASGRO recommended values. This seems to indicate that NASGRO's $\Delta K_{th}(R)$ estimates are not so good for the tested Al alloy. Its recommended toughness value $K_c \cong 730\ \text{MPa}\sqrt{\text{mm}} \cong 23\ \text{MPa}\sqrt{\text{m}}$ is about 10% lower than the measured one, $K_c = 25.4\ \text{MPa}\sqrt{\text{m}}$, a small difference that does not affect phase I FCG rates and has little effect on phase II FCG as well. The effect of the two constraint factors numerically tested in the simulations, $\alpha = 2$ or $\alpha = 3$, is relatively low at $R = 0.1$ and negligible at $R = 0.7$, when the crack closure effect is expected to be low or even negligible anyway. Finally, even though NASGRO recommends a constraint factor $\alpha = 2$ for this Al alloy, the best SYM estimates are obtained using a higher value $\alpha = 3$, the value expected from the $\alpha = 1/(1-2\nu)$ theoretically predicted for *pl*-ε FCG conditions, since Al alloys have $\nu \cong 1/3$.

Figs. 12 and 13 show the $da/dN \times \Delta K$ data points and the curves predicted by the SY-CDMs for the 7075-T6 Al alloy tested under $R = 0.1$ and $R = 0.7$ using the εN damage induced by the cyclic strain fields generated by SYM's displacement fields, and Coffin-Manson, Morrow EP, or SWT εN rules. Recall that the SY-CDMs use only the plastic part of those εN rules. This simplification is necessary, since the SYM numerical procedures discretize the *pz* ahead of the crack tip using rigid-perfectly-plastic VE elements. Recall as well that C&M does not recognize mean or peak stress effects, whereas Morrow EP and SWT do. These figures also show the original CDM + C&P and the SYM–A FCG curves with $\alpha = 3$, which yield the better predictions in Figs. 10 and 11. The FCG rates estimated by the modified CDM + C&M are essentially equal to the ones generated from the original CDM + C&P, yielding FCG curves that are quite reasonable for $R = 0.1$, albeit not as good for $R = 0.7$. This coincidence could not be anticipated, since original CDMs calculate damage accumulated by displaced HRR cyclic fields, whereas the modified CDMs use the cyclic strain field estimated from SYM's displacements along the *pz*, considering possible crack closure effects.

Although this coincidence certainly cannot be generalized, it may be seen as an indication that both procedures are at least coherent, a reassuring evidence. Finally, the SY-CDM based on Morrow EP resulted in too conservative predictions for both R levels, except for very low ΔK values near the FCG threshold, associated with low phase I FCG rates. The SY-CDM based on SWT, on the other hand, yielded intermediate FCG predictions

Figs. 14 and 15 depict the measured $da/dN \times \Delta K$ points and the FCG curves predicted by the original CDMs and by the SYMs for the 1020 steel tested under $R = 0.1$ and $R = 0.7$, respectively. Due to the high toughness of this steel, such data points cover only its phase I and II FCG behavior. The FCG curves estimated from the strip-yield

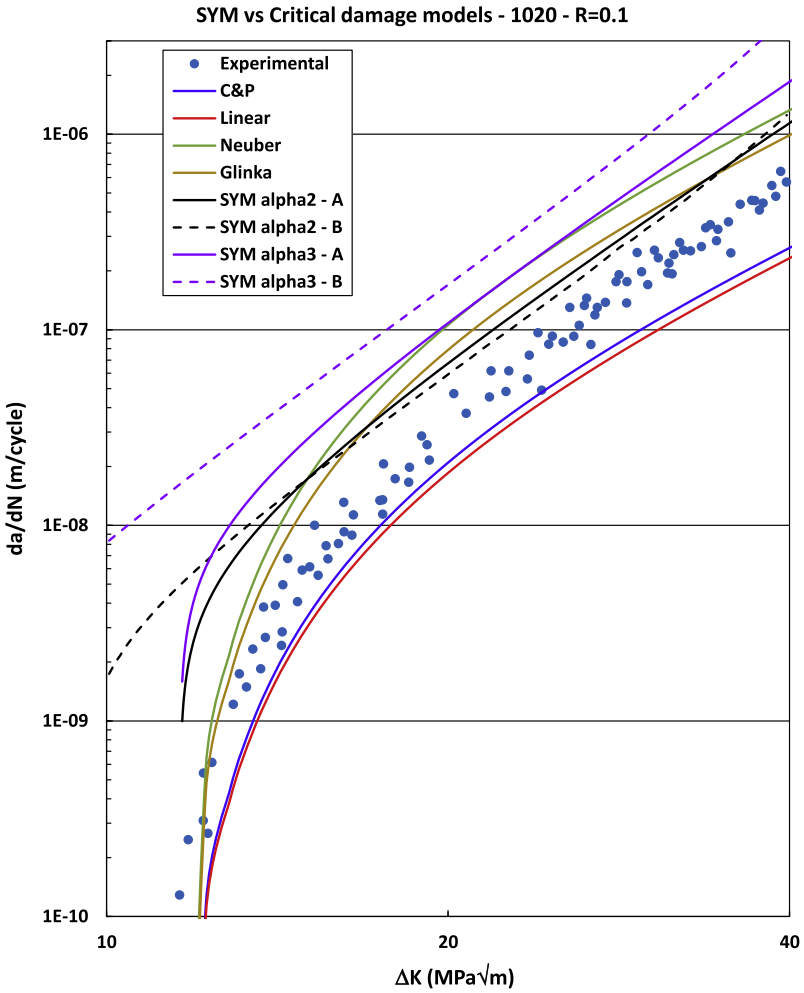

Fig. 14. SYM and original CDM estimates for the FCG curve of the 1020 steel at $R = 0.1$.

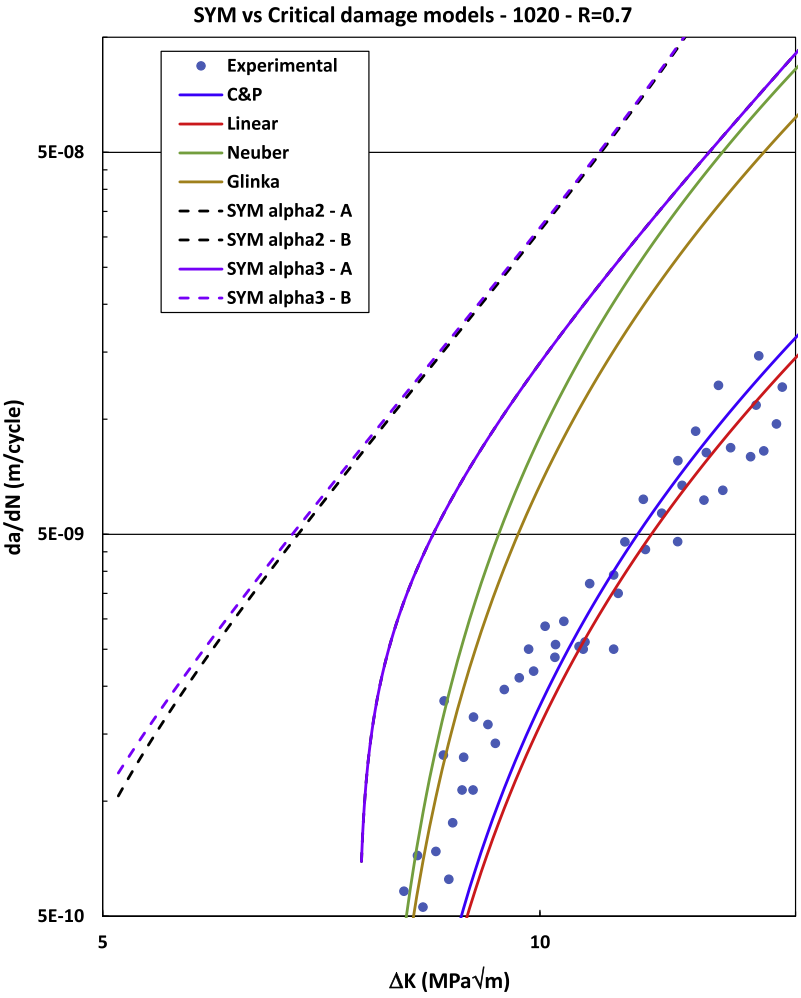

Fig. 15. SYM and original CDM estimates for the FCG curve of the 1020 steel at $R = 0.7$.

models are once again obtained using two constraint factors, $\alpha = 2$ and $\alpha = 3$, even though NASGRO recommends $\alpha = 2.5$ for this steel (assuming it has $\nu = 0.29$, the ideal value for *pl*-ε FCG conditions is, in theory, $\alpha = 1/(1-2\nu) \cong 2.38$).

The SYM−A uses measured ΔK_{th} and K_c values listed in Table 1, while SYM−B uses ΔK_{th} from Table 2. SYM−B yielded too conservative FCG curves particularly at $R = 0.7$, and for both R-ratios it did not even reproduce the shape of the measured data points. This performance may be an indication that NASGRO's $\Delta K_{th}(R)$ estimates are not so good for the tested steel either. The α-factor had the same effect as observed for the 7075 Al with $\alpha = 2$, yielding less conservative results than $\alpha = 3$. The condition A with $\alpha = 2$ produced good results for $R = 0.1$, deviating from the measured data at phase I. For $R = 0.7$ its estimates are probably too conservative for any practical use.

As expected for fatigue cracks that grow under *pl*-ε conditions, the C&P and the Linear CDMs estimate better FCG curves (as compared with the experimentally measured data) than the Neuber and the M&G models, but they are slightly non-conservative at $R = 0.1$. However, their predictions are quite good for $R = 0.7$. Neuber and M&G predicted conservative FCG rates for both R, with the latter being less conservative than the former, as expected.

Figs. 16 and 17 show the measured $da/dN \times \Delta K$ data points and the curves predicted by the SY-CDMs for the 1020 steel tested under $R = 0.1$ and $R = 0.7$, respectively. Recall that these FCG curves are generated by damage accumulation along cyclic strain fields numerically estimated by SYM procedures based on strains generated by the Dugdale-Baremblat strip-yield model but, which consider but do not use Elber's PICC ideas. Instead they calculate damage ahead of the crack tip, using Coffin-Manson, Morrow EP, or SWT εN rules, without adjustable da/dN constants.

Whereas the original CDM + C&P reproduced relatively well the data trend but yielded slightly non-conservative FCG estimates at $R = 0.1$, the SYM had a similar performance but generated slightly conservative predictions. The SY-CDMs predicted too conservative FCG rates at phase II. For $R = 0.7$, the SY-CDMs and also the SYM were too conservative, contrasting with the quite reasonable performance of the original CDM + C&P curve. Once again, the reasonable performance of *pl*-ε CDMs FCG rate estimations for this steel, which are based only on εN properties without any data-fitting parameter, certainly is no coincidence. One of the reasons for the conservative values for the SY-CDMs (Figs. 12, 13, 16 and 17) probably is the simplification of the strip-yield material behavior, assumed as rigid-perfectly-plastic. The strain hardening exponent (h) for the tested 7075 aluminum is 0.09 and for the 1020 steel 0.18, as shown in [25]. The SYM uses the flow stress in order to consider some material strain hardening, but it seems that this approach does not work well for materials with high strain hardening exponents like the 1020 steel. Damage predicted by Morrow and by SWT have other error sources, namely the average and the maximum element stresses. The SYM uses a constraint factor to deal with plane strain conditions, elevating the element tensile stress by a value of up to 3. But this hypothesis, which affects the plastic zone size, cannot be used to estimate the actual element

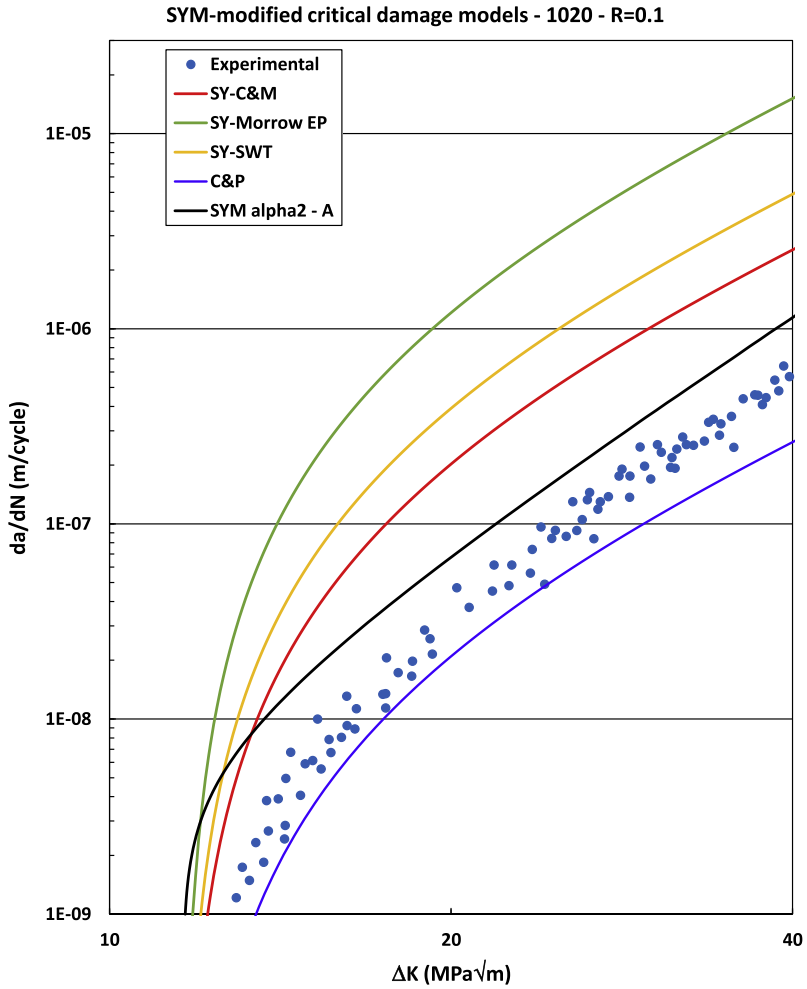

Fig. 16. SYM and SY-CDM estimates for the FCG curve of the 1020 steel at $R = 0.1$.

stress. The maximum stress ($\alpha.S_F$) is 1611 MPa for the 7075 Al and 776 MPa for the 1020 steel, and both stresses are almost twice the ultimate material strength (see Table 1). Therefore, the range of displacements estimated by the strip-yield and the strain range used by the SY-CDMs could be reduced if a more realistic material model was used to consider its strain hardening behavior. This work is in progress and will be reported soon.

In summary, in this work the very same SYM mechanics used to estimate crack opening loads in traditional strip-yield FCG models, which is based on non-singular Dugdale-Baremblat's displacement fields, is used as well to describe the EP cyclic strain fields ahead of the crack tip. This mechanics is then used to estimate FCG curves using two completely different hypotheses: (i) assuming FCG is controlled by Elber's ΔK_{eff} concepts, and (ii) supposing instead that the FCG behavior is caused by damage accumulation ahead of the crack tip, due to the cyclic stress and strain fields that act there. When properly applied, as discussed above, the better estimates generated by these very different ideas reproduced reasonably well FCG data measured under two very different $R = 0.1$ and $R = 0.7$ conditions for two materials: a low-strength 1020 steel and a high-strength 7075-T6 Al alloy. However, an important difference between the SYM and the CDM techniques must be emphasized: while the CDM requires only measurable εN properties and needs no additional data-fitting parameters to estimate the FCG behavior, the SYM estimates use at least four data-fitting parameters to achieve similar results. Notice that the SYMs estimates for the FCG behavior described in this work use listed parameters (Table 2) instead of parameters properly fitted to the measured $da/dN \times \Delta K$ curves, to guarantee a fair comparison with similar CDMs estimates. In fact, otherwise the SYM calculations could not be called *estimates*. However, under the same fairness principles, two sets of SYM estimates have been performed, SYM−A made using measured $\Delta K_{th}(R)$ and K_c values, since CDMs estimates use them as well, and SYM−B estimates made using only listed properties. It is no surprise that the former had a better performance.

The CDM procedures used here are relatively simple, since they use a reasonable FCG rule to describe the entire sigmoidal shape of typical FCG curves. In this sense, this model cannot be called entirely crack initiation-based, since it would be better to avoid such a trick. However, since the SYM procedures use the same trick, only changing the chosen FCG rule, the comparison among their predictions certainly is a fair game. It would be better to avoid such a trick altogether, but this would require a CDM based not only on an εN rule that recognizes a fatigue limit, since otherwise it would not be possible to predict a FCG threshold. It would also require a very good description of the residual stress/strain fields ahead of the crack tip. However, these points are considered beyond the scope of this article, and are left to be properly discussed in future works, which will deal with the modeling of FCG under VAL conditions.

Finally, an additional point must be emphasized: the results presented here also indicate that a good description of some experimental data is *not* a conclusive proof of any model suitability, let alone of its prevalence. What is really important when dis-

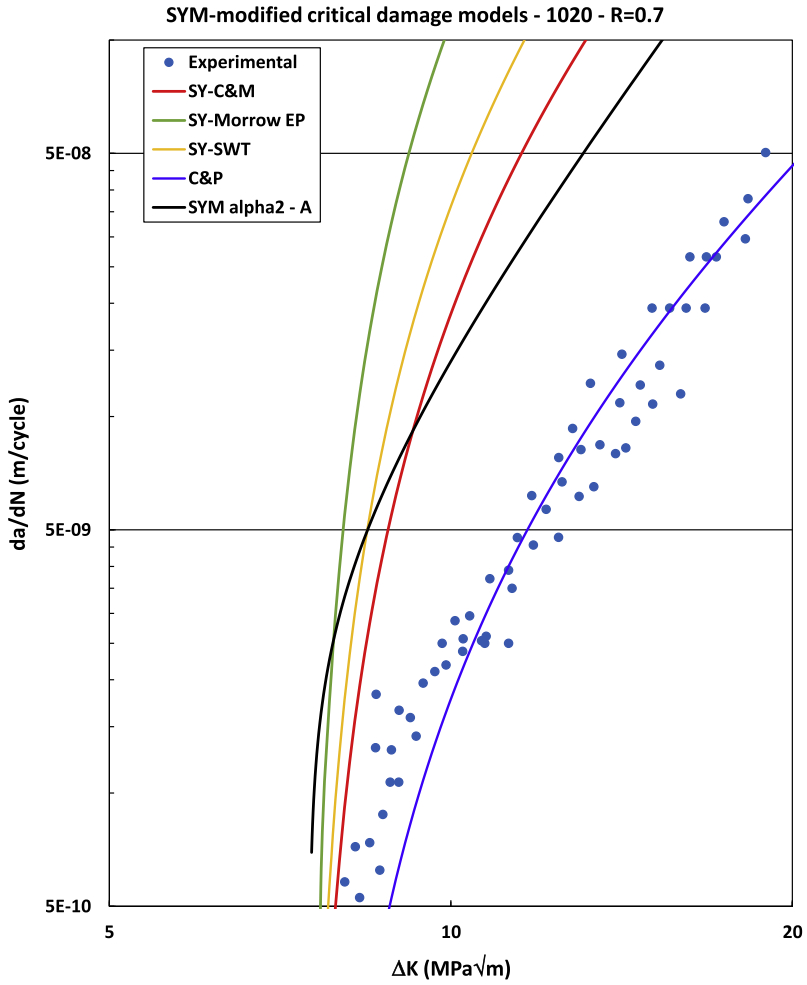

Fig. 17. SYM and SY-CDM estimates for the FCG curve of the 1020 steel at $R = 0.7$.

cussing such points is to clearly identify which set of properly measured experimental data any given FCG model *cannot* describe well. Since after so many years there is still no consensus about such questions, not even about which are the true fatigue crack driving forces, the authors hope this relatively straightforward modeling exercise can contribute at least to avoid the radical opinions that are still too common in this field.

6. Conclusions

Critical damage models (CDMs) and strip-yield models (SYMs) are used here to estimate $da/dN \times \Delta K$ curves of two materials tested under two very different R-ratios. These models are based on very different hypotheses about the cause for the FCG behavior. Whereas SYMs assume FCG is driven by ΔK_{eff}, so it depends on the interference of the plastic wakes left behind the crack tip along the crack surfaces, CDMs suppose fatigue cracks propagate by sequentially breaking volume elements ahead of the crack tip, because they accumulate all the fatigue damage they could sustain. To compare the predictions of such so different models, both types were applied to describe the properly measured FCG behavior of a 7075-T6 Al alloy and a 1020 AISI steel, whose $da/dN \times \Delta K$ curves were experimentally obtained following standard ASTM E647 procedures. Moreover, the εN properties of such materials were also measured by standard ASTM E606 procedures. The FCG and the crack initiation properties were measured in coupons machined from the same material lot, to avoid any inconsistency in the data. Both the original CDM and SYM FCG estimates predict reasonably well the measured data. Notice that the word prediction can be used with these models, since they do not need to fit the measured data. However, to properly compare them, the CDM was modified to use SYM–predicted strain fields ahead of the crack tip, which consider possible K_{op} effects but do not need them or even to adopt Elber's PICC ΔK_{eff} hypothesis to estimate FCG rates. The SY-CDM estimates proposed here also describe reasonably well the measured $da/dN \times \Delta K$ data. This indicates that, although apparently contradictory, such models are not incompatible. Moreover, the quite good performance of their predictions, especially for the 7075 aluminum, also indicates that the good fitting of some properly obtained data set is not enough to prove which one is the best. Hence, both should be considered as viable options to model the FCG behavior.

References

[1] Paris PC, Erdogan F. A critical analysis of crack propagation laws. J Basic Eng 1963;85:528–34.
[2] Castro JTP, Meggiolaro MA. Fatigue design techniques, vol. 3: crack propagation, temperature and statistical effects. CreateSpace; 2016.
[3] Elber W. Fatigue crack closure under cyclic tension. Eng Fract Mech 1970;2:37–45.
[4] Elber W. The significance of fatigue crack closure. Damage Toler Aircraft Struct, ASTM STP 1971;486:230–42.
[5] Dill HD, Saff CR. Spectrum crack growth prediction method based on crack surface displacement and contact analyses. Fatigue Crack Growth Under Spectr Loads, ASTM STP 1976;595:306–19.

[6] Newman Jr JC. A crack-closure model for predicting fatigue crack growth under aircraft spectrum loading. Methods Models Predict Fatigue Crack Growth Under Random Load, ASTM STP 1981;748:53–84.
[7] de Koning AU, Liefting G. Analysis of crack opening behavior by application of a discretized strip yield model. Mech Fatigue Crack Clos, ASTM STP 1988;982:437–58.
[8] Wang GS, Blom AF. A strip model for fatigue crack growth predictions under general load conditions. Eng Fract Mech 1991;40:507–33.
[9] Beretta S, Carboni M. A strip-yield algorithm for the analysis of closure evaluation near the crack tip. Eng Fract Mech 2005;72:1222–37.
[10] Kemp PMJ. Fatigue crack closure – a review. TR90046, Royal Aerospace Establishment, UK; 1990.
[11] Skorupa M. Load interaction effects during fatigue crack growth under variable amplitude loading - a literature review - part I: empirical trends. Fatigue Fract Eng Mater Struct 1998;21:987–1006.
[12] Skorupa M. Load interaction effects during fatigue crack Growth under variable amplitude loading - a literature review - part II: qualitative interpretation. Fatigue Fract Eng Mater Struct 1999;22:905–26.
[13] Castro JTP, Meggiolaro MA, Miranda ACO. Singular and non-singular approaches for predicting fatigue crack growth behavior. Int J Fatigue 2005;27:1366–88.
[14] Castro JTP, Meggiolaro MA, González JAO. Can ΔK_{eff} be assumed as the driving force for fatigue crack growth? Fratt Integr Strutt 2015;33:97–104.
[16] Chen DL, Weiss B, Stickler R. The effective fatigue threshold: significance of the loading cycle below the crack opening load. Int J Fatigue 1994;16:485–91.
[17] Vasudevan AK, Sadananda K, Holtz RL. Analysis of vacuum fatigue crack growth results and its implications. Int J Fatigue 2005;27:1519–29.
[18] Davidson DL, Hudak Jr. SJ. Alterations in crack-tip deformation during variable-amplitude fatigue crack growth. In: Fracture mechanics - 18th symposium, ASTM STP 945; 1988. p. 934–54
[19] Vasudevan AK, Sadananda K, Louat N. Reconsideration of fatigue crack closure. Scripta Metall Mater 1992;27:1663–78.
[20] Toyosada M, Niwa T. The significance of RPG load for fatigue crack propagation and the development of a compliance measuring system. Int J Fatigue 1994;67:217–30.
[21] Vasudevan AK, Sadananda K, Louat N. A review of crack closure, fatigue crack threshold and related phenomena. Mater Sci Eng 1994;188A:1–22.
[22] Lang M. Description of load interaction effects by the ΔK_{eff} concept. Adv Fatigue Crack Clos Meas Anal, ASTM STP 1999;1343:207–23.
[23] Dinda S, Kujawski D. Correlation and prediction of fatigue crack growth for different R-ratios using K_{max} and ΔK^{+} parameters. Eng Fract Mech 2004;71:1779–90.
[24] Castro JTP, Kenedi PP. Prediction of fatigue crack growth rates departing from Coffin-Manson concepts. J Braz Soc Mech Sci Eng 1995;17:292–303 [in Portuguese].
[25] Durán JAR, Castro JTP, Payão Filho JC. Fatigue crack propagation prediction by cyclic plasticity damage accumulation models. Fatigue Fract Eng Mater Struct 2003;26:137–50.
[26] Castro JTP, Meggiolaro MA, Miranda ACO. Fatigue crack growth predictions based on damage accumulation calculations ahead of the crack tip. Comput Mat Sci 2009;46:115–23.
[27] Majumdar S, Morrow JD. Correlation between fatigue crack propagation and low cycle fatigue properties. Fract Toughness Slow-Stable Crack, ASTM STP 1974;559:159–82.
[28] Schwalbe KH. Comparison of several fatigue crack propagation laws with experimental results. Eng Fract Mech 1974;6:325–41.
[29] Glinka G. A notch stress-strain analysis approach to fatigue crack growth. Eng Fract Mech 1985;21:245–61.
[30] Noroozi AH, Glinka G, Lambert S. A study of the stress ratio effects on fatigue crack growth using the unified two-parameters fatigue crack growth driving force. Int J Fatigue 2007;29:1616–34.
[31] Willenborg J, Engle RM, Wood HA. Crack growth retardation model using an effective stress concept. Wright Patterson Air Force Laboratory; 1971.
[32] Chang JB, Engle RM. Improved damage-tolerance analysis methodology. J Aircraft 1984;21:722–30.
[33] Withers PJ, Lopez-Crespo P, Mostafavi M, Steuwer A, Kelleher JF, Buslaps T. 2D mapping of plane stress crack-tip fields following an overload. Fratt Integr Strutt 2015;33:151–8.
[34] Kujawski D. ΔK_{eff} parameter under re-examination. Int J Fatigue 2003;25:793–800.
[35] Rice JR, Rosengren GF. Plane strain deformation near a crack tip in a power-law hardening material. J Mech Phys Solids 1968;16:1–12.
[36] Hutchinson JW. Singular behavior at the end of a tensile crack tip in a hardening material. J Mech Phys Solids 1968;16:13–31.
[37] Creager M, Paris PC. Elastic field equations for blunt cracks with reference to stress corrosion cracking. Int J Fract Mech 1967;3:247–52.
[38] Dugdale DS. Yielding of sheets containing slits. J Mech Phys Solids 1960;8:100–4.
[39] Barenblatt GI. The mathematical theory of equilibrium cracks in brittle fracture. Adv Appl Mech 1962;7:55–192.
[40] Newman JC. FASTRAN II: a fatigue crack growth structural analysis program, NASA Technical Memorandum 104159, LRC Hampton; 1992.
[41] NASGRO – Fracture mechanics and fatigue crack growth analysis software, reference manual, version 4.02; 2002.
[42] Vasudevan AK, Sadananda K, Holtz RL. Unified approach to fatigue damage evaluation. NRL Rev 2003:51–7.
[43] Rice JR. Mechanics of crack tip deformation and extension by fatigue. Fatigue Crack Propaga, ASTM STP 1967;415:247–311.
[44] Meggiolaro MA, Castro JTP. Statistical evaluation of strain-life fatigue crack initiation predictions. Int J Fatigue 2004;26:463–76.